Czech Technical University in Prague
Faculty of Electrical Engineering
Department of Electromagnetic Field

Wireless Communication System for Submucosal Implants

Master's Thesis

Bc. Marek Novák

Study programme: Electronics and Communication
Branch: Radio and optical technology
Supervisor: Ing. Pavel Puričer

Prague, May 2018

Statutory declaration

I hereby declare on my honour that this diploma thesis has been independently prepared, solely with support of the listed literature references, and that no information has been presented that has not been officially acknowledged.

Prague, 23rd May 2018 …….

Bc. Marek Novák

Acknowledgements

Foremost, I would like to express my sincere gratitude to my thesis advisor Ing. Pavel Puričer for his support of my diploma thesis, for his motivation and immense knowledge. His guidance helped me in all the time of development and writing this thesis.

Besides my advisor, I would like to thank MUDr. Jan Hajer, Ph.D. and doc. MUDr. Jan Polák, Ph.D., MBA for introducing me to medical research. Their help and assistance from medical point of view as well as the opportunity to perform my research in their labs is invaluable.

Finally, I would like to thank my parents, Irena Nováková and Vladimír Novák, for their love and unconditional support.

1 Abstract

Gastroesophageal reflux disease (GERD) and gastroparesis are two diseases of gastrointestinal tract (GIT) which can be characterized by the disorder of muscle tissue. In GERD, the lower esophageal sphincter does not close properly, allowing the acidic contents of stomach to enter esophagus. Gastroparesis is characterized by partial paralysis of stomach, resulting in food remaining there for an abnormally long time. Treatment for these diseases includes medication and invasive surgery which is dangerous. In recent years, endoscopy is getting attention because it is virtually non-invasive technique for surgeries inside GIT.

The goal of this thesis is the development of wireless link for an active implantable medical device (AIMD) which could be used in treatment of GERD and gastroparesis. The device is implanted using a technique called endoscopic submucosal pocketing. Focus is given to the design of the wireless communication link which is operated in MEDS band. Convolutional coding and encryption is developed and implemented in the system.

A prototype of AIMD with biocompatible housing and a receiver/charger device was developed and the proposed bidirectional wireless communication link was implemented using C language, PIC microcontrollers and Si4455 radio transceivers. Finally, the device was implanted into submucosa of a pig stomach with an endoscope to test the feasibility of using the device during ongoing research.

Keywords: Implantable medical device, endoscopy, submucosa, wireless link

2 Abstrakt

Refluxní choroba jícnu (GERD) a gastroparéza jsou dvě nemoci gastrointestinálního traktu (GIT), které můžou být charakterizovány nedostatečnou funkcí příslušné svaloviny. U refluxní choroby jícnu nedochází k uzávěru dolnojícnového svěrače, což umožňuje vstup kyselého obsahu žaludku do jícnu. Gastroparéza je charakteristická částečnou paralýzou žaludku, což vede k tomu, že potrava v něm zůstává po dobu delší, než je běžné. Léčba těchto onemocnění je zpravidla medikamentózní nebo chirurgická, která s sebou nese zvýšená rizika. Endoskopie zažívá v posledních letech zvýšený zájem, protože se jedná o téměř neinvazivní techniku pro zákroky v GIT.

Cilem této diplomové práce je vývoj bezdrátového rozhraní pro aktivní implantabilní zdravotnický prostředek (AIMD), který by mohl být použit pro léčbu GERD a gastroparézy. Zařízení je implantováno technikou, která se nazývá „endoscopic submucosal pocketing“. Práce je specificky zaměřena na vývoj bezdrátového komunikačního rozhraní provozovaného v pásmu MEDS. Konvoluční kodování a šifrování je vyvinuto a implementováno.

Prototyp AIMD s biokompatibilním obalem a zařízením pro příjem dat a nabíjením bylo vyvinuto a navržený obousměrný bezdrátový komunikační řetězec byl implementován v jazyce C s použitím mikrokontrolerů PIC a Si4455 radiového transceiveru. Nakonec bylo zařízení otestováno jeho implantací do submukozy v prasečím žaludku pomocí endoskopu, čímž byla otestována možnost jeho využití v navazujícím výzkumu.

Klíčová slova: Implantabilní zdravotnický prostředek, endoskopie, submukoza, bezdrátový spoj

3 Table of contents

3.1 List of figures

3.2 List of appendices

Appendix 1: Layout of printed circuit boards

3.3 List of abbreviations

ADC	Analog-to-digital converter
AFA	Adaptive frequency agility
AIMD	Active implantable medical device
AMI	Active medical implants
ASIC	Application-specific integrated circuit
BGA	Ball-grid array
BOM	Bill of materials
CSP	Chip-scale package
CTS	Clear to send
DAC	Digital-to-analog converter
ENIG	Electroless nickel immersion gold
ETSI	European Telecommunications Standards Institute
GIT	Gastrointestinal tract
HSS	High-speed steel
LBT	Listen before talk
MICS	Medical Implant Communication Service
OOK	On-off keying
PPI	Proton pump inhibitors
QMS	Quality management system

4 Introduction

In past few decades, the miniaturization of electronics empowered the innovation in all aspects of our lives – the size of devices and electronic packaging is getting smaller while the computing power and number of features goes exponentially up. Radio circuits in mobile phones which were, in not very distant past, realized semi-discrete with bulky LC filter networks are now integrated in a single RF SoC. This miniaturization has affected the human lives, from consumer electronics through automotive to medical devices. The latter is a very specific area. Although the innovation in medical devices industry, especially active implantable devices, is slower due to the high-reliability requirements of these instruments, new techniques and devices are constantly developed. New medical devices are required to be developed under QMS (quality management system) for medical devices development and manufacturing, full clinical trials or equivalency assessment must be completed to pass the process of certification of new types of devices and the whole supply chain needs to be tracked. AIMD like pacemakers are expected to stay safely in the body for at least 10 years. This poses challenges not only from electronics point of view but also mechanical point of view as regular plastic materials often cannot be used because plastic materials are very permeable to water and oxygen. Biocompatibility is a key requirement. Human body's immune system will reject any object which is not designed with biocompatibility in mind. One of the most ambitious and quickly developing areas of surgery is endoscopy. This surgery technique uses an electromechanical instrument which is mechanically controlled from outside of the body by hands of the surgeon and it allows to perform various procedures inside of GIT.

This thesis will focus specifically on development and design of secure radio link between a prototype of implantable medical device and device which will be placed outside of the body. The radio link will be developed in accordance with frequency bands allocated to AIMD and other requirements stated by ETSI standards.

5 Novel endoscopic techniques

Endoscopy is a mini-invasive surgical method used primarily for procedures and treatment carried out in GIT. The endoscope is inserted either per oral to access esophagus, stomach and duodenum or per anus to access the colon. The endoscope[1] is an instrument which is used to carry out the procedure. It consists of a "tower" which contains the electronics instruments containing power and data buses for the connection of the endoscope as well as liquid media pumps. The endoscope can be divided into three main portions – the "connector" which connects to the tower, a controller which is used by the endoscopist to control the device and the tube with bending section which is inserted in the body. The diameter of the insertion tube is about 1 cm and contains data and power buses to the open end which embeds a camera, light source and channels through which the endoscopist may insert various tools like grasper tools, haemostatic clips, needles, knives etc.

Virtually all tubular organs in human body consist of five main distinctive layers. The outside layer is either serosa or adventitia (serosa only covers the organ, adventitia is connective tissue which binds to adjacent tissues and organs). Then the longitudinal and circular muscle layer follows. In the virtual middle of the wall of the organ, the submucosa is located. Submucosa is a semi-rigid layer of tissue which contains blood vessels. The inner layer is mucosa which is exposed to the inner volume of the organ.

A method which will be exploited in this thesis is called ESP[2]. This technique is today primarily used for techniques like POEM[3]. However, this space is very specific in its location. It is located in between a muscular layer which can be electrically stimulated and the inner mucosa layer which has access to the inside of the organ. If an active implantable device could be inserted to the submucosa, it could serve as a neurostimulator, sensor or both. First successful implantation of an object into submucosa was reported in 2012[2]. The successful implantation of an active battery-powered neurostimulator was published by Dr. Hajer and the author of this thesis in 2017[4]. This thesis further builds on this previous work. The wireless link in the published implant was not in accordance with valid regulations concerning AIMD (discussed in detail in section 6). Also, it was not wireless powered. The battery size was extremely limited by the maximum size of the implant which was implantable into submucosa which was a cylinder with diameter of 22 mm and thickness of 5 mm. The maximum life-time of the implant was few months at most with minimal number of neurostimulation cycles. The material was not biocompatible so the experiments which can be performed with such implants are experiments on animal models (artificial or extracted organs) and non-survival models (the animal under anaesthesia is living during the surgery and is euthanized right after the surgery).

First, the location of the device inside esophagus or stomach is determined visually. After that, an injection with physiological solution with methylene blue is injected into the submucosa[4]. This dilates the submucosa and colours the tissue in blue. Only the submucosa is coloured due to its

porous and gel-like behaviour. Lower and upper layers are not coloured. This serves as an indicator for the endoscopist to avoid the penetration of outer or inner layer of the organ from the submucosa. Then an incision with endoscopical knife is performed to access the submucosa. Then the surgical knife is inserted into the incision and the pocket in the submucosa is further dilated and expanded to accommodate the device to be implanted. Finally, the device is inserted into the newly formed submucosal pocket and the pocket is closed using either haemostatic clips or more advanced instruments like OVESCO (OVEr-the-SCOpe clip).

This technique will be used in this thesis to test the feasibility of the developed device to be securely implanted into the submucosa which is one of the basic requirements.

6 Gastroesophageal reflux disease and gastroparesis

Both GERD[5] and gastroparesis[6] are diseases of the GIT characterized by malfunction of the muscle tissue. The GERD which is also known as acid reflux is a condition where acidic contents from the stomach enter the esophagus due to the inability of lower gastroesophageal sphincter to close properly. Under normal conditions, this sphincter is closed unless the food is passed through the esophagus into the stomach. There are four main ways of treatment[5] of GERD. The least invasive way is to adjust the diet and lifestyle – e.g. not lying down for several hours after eating and avoiding certain food. Medication – mainly proton pump inhibitors (PPI) can be used as well. The invasive ways of treatment of GERD are a surgery or implantation of electrostimulation apparatus which stimulates the lower esophageal sphincter. This invasive method of treatment is currently very risky and is performed only in cases when the conservative treatment failed to alleviate of the symptoms. Currently there is one AIMD which is used for treatment of GERD which uses electrical stimulation – Endostim[7]. This device resembles a standard cardiac stimulator and is placed subcutaneously with leads connected to the esophageal sphincter.

Gastroparesis[6] is, compared to GERD which affects about 15 % of population[5], a relatively rare disease. It is characterized by a partial paralysis of the stomach which results in the inability of the stomach to empty properly. Treatment is done with medication or surgery. There is one neurostimulation device – Medtronic Enterra II[8] – currently on the market which is designed specifically for the treatment of gastroparesis. It is similar to the Endostim stimulator, its construction is very similar to a cardiac neurostimulator. It is placed subcutaneously with electrodes inserted into the outer wall of the stomach.

Risks associated with both Endostim and Enterra II are a requirement of full anaesthesia and risk of the leads penetrating either the esophagus or stomach[9] which is a life-threatening situation. Thus, moving the electrical neurostimulation inside of the esophagus or stomach without the requirement of highly invasive procedure is a next logical step in making the treatment more accessible and much safer than current techniques.

7 Legal analysis – radio links for AIMD

Note: The wireless communication link which is developed in this thesis is developed in accordance to laws and legal requirements of European Union at the time of writing of this thesis. FCC information about AIMD wireless links is provided for sake of completeness.

The main authority for allocation of radio spectrum and standards for ICT in European Union is the European Telecommunications Standards Institute (ETSI). The standards produced by this standardization organization include consumer short-range devices as well as specialized standards for AIMD.

The building of a framework for AIMD was initiated in 1999 by Medtronic Inc. by submitting a petition to FCC[10]. Shortly after that, the Medical Implant Communication Service (MICS) was established and extended. It is set aside 402 - 405 MHz band and is designated for a very low EIRP of only -16 dBm to avoid interference with other users using same technology. Before this, only inductive communication systems were allowed to be used in AIMDs to communicate with devices outside of the patient's body. The number of channels which were assigned to this band was ten, each 300 kHz wide. This spectrum can be used both for uplink and downlink. Typical use cases are sending telemetry data from the AIMD to external programmer, sending instructions to the AIMD or updating the firmware of the AIMD by the external programmer.

In 2006, FCC decided to further expand the frequency bands. Currently, almost 30 MHz of spectrum within 401 to 457 MHz is reserved for AIMDs. ETSI, on the other hand, harmonized only 401 to 402 MHz and 405 to 406 MHz together with the original MICS band (MedRadio band). In addition, a part of spectrum within 2.4 GHz ISM band was allocated to low power medical implants.

The essential requirements and safety of medical devices are covered in IEC 60601[11] which is a series of standards. These requirements are covering mechanical and electrical properties of medical devices. According to 93/42/EEC directive[12], AIMDs are considered a class III medical device. While class I is a medical device which does not require the manufacturer to submit the documentation to a notified body for assessment while class II and class III are required to. Standards for wireless communication systems in AIMDs in 400 MHz band are covered in EN 302 537, EN 301 839 and EN 302 537-1. For further research, a frequency band of 402 to 405 MHz will be evaluated, and the radio link developed in this thesis will maximally conform to the requirements stated in EN 301 839.

The standards cover the requirements on frequency allocation, maximum channel width, interference mitigation, maximum duty cycle and other parameters. As for the transmitter, the frequency error of the equipment shall not exceed 100 ppm under any condition. The maximum allowable emission bandwidth is 300 kHz except for maintaining a communication session when

more than 300 kHz may be used. All emissions outside of the band should be attenuated at least 20 dB from other channels. The effective radiated power of AMI (active medical implants) which uses LBT (listen before talk) and AFA (adaptive frequency agility) shall not exceed 25 μW ERP. For systems which do not use LBT and AFA, the transmit power shall not exceed 100 nW and the duty cycle is limited to 0.01 %. Spurious emissions of the transmitter are extremely limited, to under 2 nW in some bands.

In the presence of blocking continuous wave at centre frequency +- 5 MHz and level 35 dB above LBT threshold, LBT threshold power level requirement should still be met. This means that the decision of LBT should not be altered by the blocking carrier.

Based on this information, following preliminary information was done to comply with the standards described above. Total of 8 channels, beginning with a channel with centre frequency of 402.150 MHz with total occupiable bandwidth of 300 kHz will be used. LBT will be implemented on both sides – receiver and transmitter, while AFA will be implemented on side of the device communicating with the implant. In the presence of blocking in current channel, the device will choose a channel which is not blocked and will transmit the new channel number to the implant through out-of-bands communication means. The transmitting power of the transmitter both in implantable device and outside device should be adjusted to be under -16 dBm EIRP. The actual output power of the implantable device may be actually larger as the antenna will be electrically small and in a proximity of battery. Similar can happen to the outside device as well.

8 Research goals

The primary goal of this research is to design a wireless link for AIMD under a large overall dimension constraint. The device shall include wireless charging capability and 402 MHz MEDS-compliant wireless communication link within dimensions which are small enough to insert the device into a pocket created into submucosa during an endoscopic procedure. Next, the wireless link should include sufficient channel encoding to avoid errors occurring during the transmission. The radio link should be also secured by encryption to avoid potential misuse. Finally, the device should be tested on either animal model or living animal to demonstrate the previously described capabilities. The enclosure of the device should provide sufficient waterproofing against neutral and acidic water-based solutions. The secondary goal is the design of biocompatible stimulation electrodes as well as two-electrode amperometric cell for measurement of bioanalytes. The bipolar neurostimulation patterns generated by the device should comply and be equal or exceed ranges defined by systems which are used today[8] – Medtronic Enterra II and Endostim. The device should be able to operate at least for 2 weeks without recharging with small dose of neurostimulation. Small dose of neurostimulation was defined as 5 second cycle, once every 60 minutes.

9 Wireless channel

In a traditional system. the properties of the wireless channel are evaluated by determining the values of active and passive elements such as antennas, cables, free space path loss, and properties of radio receiver and transmitter such as output power and receiver sensitivity. Then, the Friis equation is used the calculate the expected loss and link margin of the system. In case of a system presented in this thesis, majority of these parameters can be only predicted with some degree of accuracy. The reasons are discussed below. A method which does not calculate the link margin precisely was developed to assess the feasibility of the wireless channel with given parameters.

The communication link will be working in 400 MHz frequency band. The boundary between near field and far field in antennas which are physically larger than a half-wavelength of the operating frequency is defined by the Fraunhofer distance. The wavelength of a 400 MHz wave is approximately 75 cm in vacuum. This indicates that both receiver and transmitter will utilize electrically small antenna. Due to this and the close proximity, the wireless link is not operating in far field. This means that the path loss cannot be calculated correctly using the free space path loss equation as the distance between antennas (usually 5 - 30 cm) will always fall within either near field or transitional field. The design of the antenna at the receiver is extremely space constrained and the antenna is placed near metallic objects (PCB with components and battery). This implicates a complex structure of EM fields which, until the final design, is hard to simulate. Thus, the most convenient ways to characterize the antenna is to use a vector network analyzer to measure the S parameters and match the antenna. Normally, electrically small antennas are not directional. Electrically small antennas are further characterized by low input resistance, high input reactance and very low radiation efficiency[13]. Surprisingly, some of those parameters can be considered desirable for the application in an AIMD. Low directivity is in fact greatly beneficial because it allows the implant and/or receiver to be placed almost in any angular direction with respect to the receiver without compromising the link quality. The low radiating efficiency of the antenna can counteract the high transmitting power of the receiver to achieve desired output power (-16 dBm for AIMDs[14]).

For estimation of the path loss, no obvious way except for full EM simulation seems to be viable. Due to the proximity of transmitting coil to the radio transceiver, the maximum communication distance between the two transceivers is never going to be larger than 20 cm (limit given by the range of wireless charging).

According to the experimental data gathered during previous experiments in past research[4], the path loss in the wireless channel at 1 meter is approximately 45 dB. A significant factor which affects the radio link is the presence of body tissue and liquids. The implantable device antenna is surrounded by a conductive environment which induces high-losses. Empirical models were already developed for the attenuation of body tissue[15].

According to the source, tissue-induced loss at 403.5 MHz is 17 to 19.2 dB for a maximum tissue thickness of 158.2 mm. Thus, the combined maximum expected loss caused by the tissue propagation and free space path loss is roughly 65 dB. Assuming the receiving antenna gain of -5 dB (it will be also electrically small and covered by hand as it will be located in the handle of the receiving device) and -30 dBm EIRP from the implantable device (-26 dBm maximum allowable EIRP and 4 dB reserve), the expected minimum power at the receiver is -95 dBm. With 5 dB overhead, the receiver sensitivity for the maximum allowed BER which will be determined in next chapter is -100 dBm. This value is realistic and the transceiver which was used can achieve this bitrate at 100+ kbps and 0.1 % BER[16]. Thus, there is potential to further lower the output power of the transmitter to reduce the power consumption, heat dissipation and heating of the tissue around the antenna.

When it comes to wireless communication, usually the most energy demanding activity is receiving mode because it must be active throughout the whole period when a new message should arrive. The transmission of the packet is not as much energy demanding as it lasts only until the packet is transmitted. However, any radio operation is power demanding because the oscillator, PLL+VCO and the mixers must be active for the whole period. In Si4455 radio transceiver which is used, the RX current is 10 mA[16]. If the implant had to be in receiving mode for the whole time, it would be extremely power demanding and the battery would practically last for less than 1 hour.

A solution was developed to solve this problem. Every communication with the implant is initiated by the charging device. The charging device can transmit an OOK (on-off keying) modulated message modulated on the magnetic field generated by the charging coil. At the beginning of the transmission, a 100 ms “logical-zero” (no magnetic field) pulse is introduced. This signalizes to the implantable device that a communication is starting. To avoid misclassification of charging cycle end as communication request, a 30 ms logical one is introduced after. Then, 8-bit cipher key and 3-bit channel ID followed by a parity bit is provided. A 30 ms period is given to the implantable device to set the transceiver up to receiving mode. After that, a 60 ms window is provided for the transceiver and charging device to exchange data. The charging device transmits a packet with configuration or a packet containing only the request for telemetry information retrieval. This packet is followed immediately after processing by the implantable device with the reply which contains the required data.

10 Source and channel coding

Source codes are used to compress naturally redundant messages for efficient transmission, while channel codes systematically add redundancy to enable high rate transmissions while minimizing the amount of errors[17]. The development of both source and channel coding started with the characterization of the amount of data which will be transmitted during a regular transmission. The purpose of the device is to transmit small amount (up to 10 bytes) of telemetry data – temperature, battery voltage, bus voltage etc. and to receive new neurostimulation settings. This data does not contain significant redundancy and any means of compression of < 12 bytes of data would be impractical and would increase the power consumption. Thus, it would not make sense to implement any type of source coding. The preamble and sync word could be longer than the payload itself.

On the other hand, channel coding adds redundant data into the message to assure error-less message transmission. The system described in this thesis represents an example of safety-critical system which comprises of an active implantable device which is intended for research purposes on living pigs to assess the feasibility of submucosal neurostimulation in treatment of gastroparesis and gastroesophageal reflux disease.

The channel code usually detects some amount of errors and may correct typically a smaller amount of errors in the sequence. These codes can be divided into two main groups – block codes and convolutional codes.

In consumer electronics, error correcting algorithms are often omitted and only an error-detecting algorithm is used. A common and widespread used algorithm is CRC[18]. It is an error detecting code to check accidental changes of the data. It is a hash function which processes a block of data and outputs a hash which can be calculated from the received data in the receiver and compared to the received CRC case. In case the received data will not yield same CRC hash, either CRC hash or message is corrupted. The fact that there is no data correction implemented means that the message would have to be retransmitted which consumes energy and allocates additional space in radio spectrum. Thus, error-correcting channel coding will be implemented.

When comparing block codes to convolutional codes[17], block codes encode one block of data at a time, independent of other blocks. The added redundancy is called “parity bits”. By calculating the syndrome, errors can be detected and after that, corrected (if the code is able to fix the amount of errors in the input string). On the other hand, in convolutional codes, code word depends on a “current” message block as well as a specified number of previous message blocks. The encoder itself has a memory. The functionality of the convolutional code may be described and visualized in diverse ways. The first way is by using generator polynomial. Every convolutional code can be defined by constraint length, rate and generator polynomial.

In this thesis, a rate ½ convolutional code with constraint length of 3 and generator polynomial of {101, 111} will be implemented because it has a low memory footprint in terms of number of states and at the same time, sources confirm it is effective in error correcting[19]. The code rate is the proportion of data which are non-redundant. That means that if for every n bits of useful information, k bits of information are generated, the code rate is n/k. The constraint length is an integer number which represents the memory of the convolutional code – on how many bits the encoder depends. If the constraint length is 3, the encoder output depends on the actual bit and 2 previous ones. The generator polynomial itself is a representation of XOR additions which result in generating of the channel symbols based on the input bit and previous bits. Another representation of the convolutional code which was beneficial in the design is the trellis. Let's assume that the coder operates in binary base and has N memory bits. The memory bits can be represented as "states" of the convolutional coder. During the encoding process, the state of the coder changes with incoming bits. The transitions between the states are well defined – in case of binary base, every state can be changed to 2 states depending on the incoming input bit. This transition will generate a group of bits generated by the encoder – in this case, two bits per one bit of input data. Each transition is uniquely defined by the actual state, final state, channel code sequence generated and symbol which is being coded.

In software, several functions were implemented in C language to accommodate the convolutional encoding and decoding process. These functions were optimized to be as RAM efficient as possible. The total amount of RAM in the used microcontrollers is less than 2 kB. First, two structs were introduced for clarity of the code:

```
typedef struct {
  uint8_t payload[12];
  uint8_t encoded[24];
} ConvPayload;

typedef struct {
  uint8_t weight[4];
  uint32_t inputword[4][3];
} ViterbiTrellis;
```

The "*ConvPayload*" struct defines the payload and is used both by convolutional coder and Viterbi decoder algorithm. The "*ViterbiTrellis*" struct is used for passing one step of Viterbi algorithm to the next step. The convolutional code which is used in this thesis was described using paths as following:

```
#define INDEX_FINALSTATE        0
#define INDEX_CODE              1
#define INDEX_SOURCESYMBOL      2
const uint8_t Viterbi_StateTransitions[8][3] = {{0,0,0},{2,3,1},
                                                {0,3,0},{2,0,1},
                                                {1,1,0},{3,2,1},
                                                {1,2,0},{3,1,1}};
```

These 8 paths represent all possible transitions between one state and another. As stated above, each transition is characterized by the source state, final state, source symbol and encoder output. The source state is defined by the integer division of the position in the array by two. The integer triplet represents (from left to right) the final state, encoder output and source symbol. The first function which was implemented was the Hamming distance function:

```
uint8_t HammingDistance(uint8_t in1, uint8_t in2) //only for 2-bit
                                                    words
{
    uint8_t res = in1 ^ in2;   //XOR to determine number of bits which
                                 are different
    if      (res==0) return 0; //simple if/else if look-up table
                                 structure to provide the result
    else if (res==3) return 2;
    else             return 1;
}
```

This function was implemented using a look-up table principle where XOR operation is performed on the data and provide a result based on an if/else if structure. This function was programmed to work only on two-bit data input to be as efficient as possible. Next, the function for convolutional encoding was implemented:

```
void Conv_Encode(uint8_t *in, uint8_t *out)
{
    uint8_t ActState = 0;
    uint8_t ActBit = 0;
    uint8_t bincr = 0;
    uint8_t cntmove = 0;

    for(uint8_t i=0;i<24;i++) //zeroing the output vector
    {
        out[i] = 0x00;
    }
    for(uint8_t i=0;i<12;i++) //for every input byte
    {
      for(uint8_t j=0;j<8;j++) //for every bit
      {
       ActBit = 0;
       if(in[i]&((0x80>>j))) ActBit = 1; //determine if the bit is 0
                                           or 1
       bincr = 0;
       if(j>3) bincr=1; //after filling the first output byte, set
                        this variable to 1
       cntmove = 6-2*(j&0x03); //determine where to place the two bits
       out[2*i+bincr] += (Viterbi_StateTransitions[(ActState<<1)+
ActBit][INDEX_CODE])<<(cntmove); //use the state transitions table to
                                    encode the message
       ActState = Viterbi_StateTransitions[(ActState<<1)+ActBit]
[INDEX_FINALSTATE]; //save current state for next cycle
      }
    }
}
```

One of the challenges of programming this function is that the encoder works bitwise but the data is saved in uint8_t array. Before the encoding process, the data must be split to individual bits and the output with double data rate needs to be saved into another uint8_t array. The beginning state is state 0. After that, the function propagates through the data bitwise and uses the state transition matrix to encode the message. The last function is the Viterbi decoder which takes the message encoded by the convolutional coder and decodes the original message from it, detecting and correcting errors during the process:

```
ViterbiTrellis ViterbiStep(ViterbiTrellis PreviousPaths, uint8_t
NewCode)
{
uint8_t NewWeight = 0;
uint8_t Code = 0;
uint8_t FinalState = 0;
uint8_t SourceSymbol = 0;
uint8_t StateOccupied = 0;
uint8_t PrevPathIndex = 0;
ViterbiTrellis OutTrellis;

    for(uint8_t i=0;i<8;i++) //for every path
    {
     PrevPathIndex = i>>1;
     Code = Viterbi_StateTransitions[i][INDEX_CODE];
     FinalState = Viterbi_StateTransitions[i][INDEX_FINALSTATE];
     SourceSymbol = Viterbi_StateTransitions[i][INDEX_SOURCESYMBOL];

     NewWeight =
PreviousPaths.weight[PrevPathIndex]+HammingDistance(NewCode,Code);
//increase the Hamming distance of the previous path by the new
Hamming path increment
     if(CheckOccupiedState(StateOccupied, FinalState)) //if the
current final state was already processed, compare if the weight of
current path is lower than the previous one and choose the lower one
     {
         if(NewWeight<OutTrellis.weight[FinalState])
         {
               OutTrellis.weight[FinalState] = NewWeight;

SetInputWord(OutTrellis.inputword[FinalState],PreviousPaths.inputword[
PrevPathIndex],SourceSymbol);
         }
     }
     else //if the final state is processed for the first time, just
write the result
     {
          OutTrellis.weight[FinalState] = NewWeight;

SetInputWord(OutTrellis.inputword[FinalState],PreviousPaths.inputword[
PrevPathIndex],SourceSymbol);
     }
     StateOccupied = UpdateOccupiedState(StateOccupied, FinalState);
    }
    return OutTrellis;
}
```

The first function performs a single step on the data. It takes the input *ViterbiTrellis* struct with data about the states and cumulative Hamming weights. After that, it evaluates all 8 transitions with respect to the received group of two bits, calculates the Hamming weights and chooses the path with lowest Hamming weight for each of four states. These four states are pushed to *OutTrellis* variable together with the message (which also cumulates from all previous steps). This step is iterated until there is no new received encoded data. After that, the path with the lowest Hamming weight is chosen. If the cumulative Hamming weight is 0, the message was received without errors. If it is non-zero, there were errors during the transmission.

Due to RAM and ROM constraints (due to the usage of a low-cost 8-bit microcontroller), one of the main challenges in the design of both convolutional coder and Viterbi decoder was the optimization of the code. The optimization is usually a trade-off between speed and RAM+ROM usage. The convolutional code itself is defined only with 24 bytes of ROM. Both convolutional coder and Viterbi decoder use the code definition array to save space. Next, a large amount of RAM was saved by letting the algorithm "forget" the old paths. In each step, there are 4 paths which enter the trellis. Those 4 paths expand to 8 paths, respective Hamming distances increment is calculated. To each state, exactly two paths compete for the lower Hamming distance value. Four paths with larger Hamming distance are discarded and the resulting four paths are the input four paths for the next step. The only problem is how to keep a record about the path as a whole. Frequently used approach is to keep track of the whole path. This would be, however, extremely RAM-consuming. Thus, each path has a memory, but it is limited just to data bits which are encoded. Thus, the total amount of RAM being occupied by the algorithm (excluding variables which are dynamically allocated in the function and discarded after execution) is 152 bytes, including the variables for storing the payload in its encoded/decoded state. The total space occupied by software (in ROM) is 1638 instructions. The total time needed for encoding of the message is 7 ms and the total time for Viterbi decoding of the message is 193 ms when the program is running on PIC16F1718 MCU at 16 MHz. Especially the decoding time is very slow but is acceptable in this stage of the project as there will be only a few packets encoded and decoded every second in worst scenario.

There are two different packet structures – one for the configuration sent from the charging device to the implantable device and another used as an acknowledge packet from the implantable device to the charger device.

```
typedef struct {
  uint8_t DeviceID[3];
  uint8_t ConfigPacket : 1;
  uint8_t :0; //7 bits reserve for flags
  uint8_t OnTime[3];
  uint8_t OffTime[3];
  uint8_t StimVoltage;
  uint8_t StimFreq;
} PayloadPacket;

typedef struct {
  uint8_t DeviceID[3];
  uint8_t Ack : 1;
  uint8_t :0; //7 bits reserve for flags
  uint8_t BatteryVoltage;
  uint8_t StimParameterCRC;
  uint8_t NotUsed[6];
} AckPacket;
```

In the packet “PayloadPacket”, the information about the address about the configuration of the neurostimulation is sent to the implantable device – on time, off time, stimulation voltage, stimulation frequency and whether the device is active or not. The acknowledge packet is used by the implantable device to send the telemetry data – battery voltage.

11 Data encryption and security

The security of the wireless link in the device is both intrinsic and implemented in software. There are two communication channels in the device, one is the bidirectional radio link operating at 400 MHz which is with no encryption and other security measures quite vulnerable to attacks. The second way of communication is downlink-only OOK modulated carrier from the charging device. This method obviously provides only one-way communication from the charger to the implantable device. However, this link is harder to be compromised because it requires direct contact with the surface of the body. Thus, the cipher key does not need to be transmitted via same channel as the data. To reduce the power consumption of the MCU, a simple XOR cipher was implemented. 8-bit cipher code is used as a seed for a pseudorandom generator which creates 12 bytes long sequence. The goal of expanding the 8-bit cipher code and not using it directly is to reduce the vulnerability of the algorithm to frequency analysis attack. Then, the convolution code encoded message is XORed with the pseudorandom generated sequence. On the receiver side, the message is then simply XORed again with the pseudorandom generated sequence to retrieve the original message.

The pseudorandom generator which was used in this project was inspired by a solution[20] which describes a pseudorandom generator specifically optimized for a 8-bit microcontroller. Other types of pseudorandom generators which are commonly used, utilize either multiplication or use variables larger than 8 bits. Every operation with multiple bytes variable consumes an excessive amount of instructions as well as program space. As this pseudorandom generator comes from an Internet source and its properties weren't published, before implementation, the basic features of the generator were tested in MATLAB. First, it was tested if it produces a uniform distribution. Next, the length of the pseudorandom sequence was tested. The distribution is in Fig 1. The length of the pseudorandom sequence was determined by generating a sequence 10^8 long. The result of *seqperiod* function returned 10^8 which means that the length of the pseudorandom sequence generated by this algorithm is equal or larger than 10^8. Given these properties, the pseudorandom algorithm can be considered good and acceptable for the use described herein. A

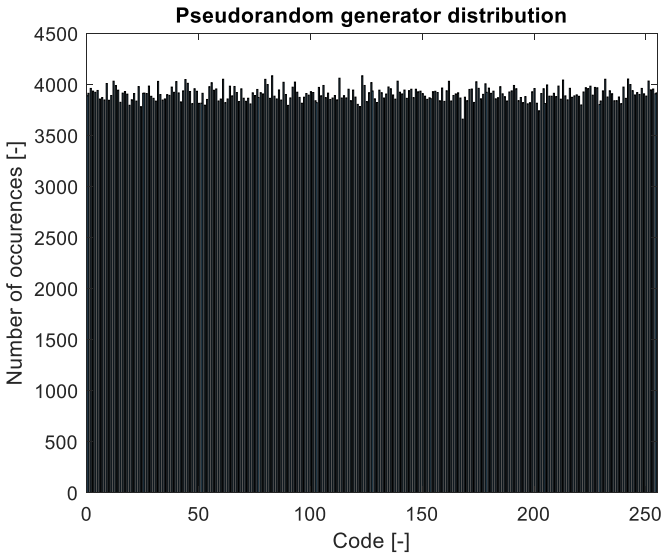

Figure 1: Pseudorandom generator distribution

seed transmitted through the inductive link is initializing the pseudorandom generator. After that, 12 bytes of pseudorandom sequence is generated and a bit XOR operation is performed on the payload. The decryption is performed the same way – the encrypted sequence is XORed with the encrypted sequence to get the original payload.

To demonstrate the importance of the pseudo-randomly generated cipher sequence and not use just the seed itself, an example is shown in Fig. 2. Especially in the acknowledge packet, half of the packet is unused. If the seed itself was used to encrypt every byte, a clear pattern would be visible.

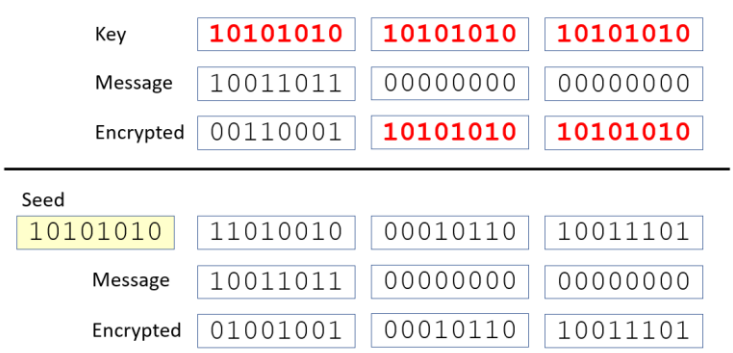

Figure 2: Comparison of encryption with and without pseudorandom generator

In fact, any byte with 0x00 value would be equal to the seed after XOR operation. The communication could be attacked very easily this way. On the other hand, when the seed is used to generate a pseudorandom sequence, this situation does not happen. It is close to the ideal Vernam cipher which, mathematically, cannot be breached[21]. In Vernam (also called one-pad) cipher, the message is XORed with a randomly generated noise. In this thesis, the noise is generated pseudorandomly from out-of-band generated seed.

The source of entropy for seed generation is the human hand input. During the button push before the transmission starts, the time for which the button was pushed is measured in approximately 10 µs increments by continuously incrementing *uint8_t* variable which also trims the output to 8 bits. This number is then used a seed which is both transmitted out-of-band and used for encryption and decryption of messages from the implantable device.

12 Visualization of the communication channel

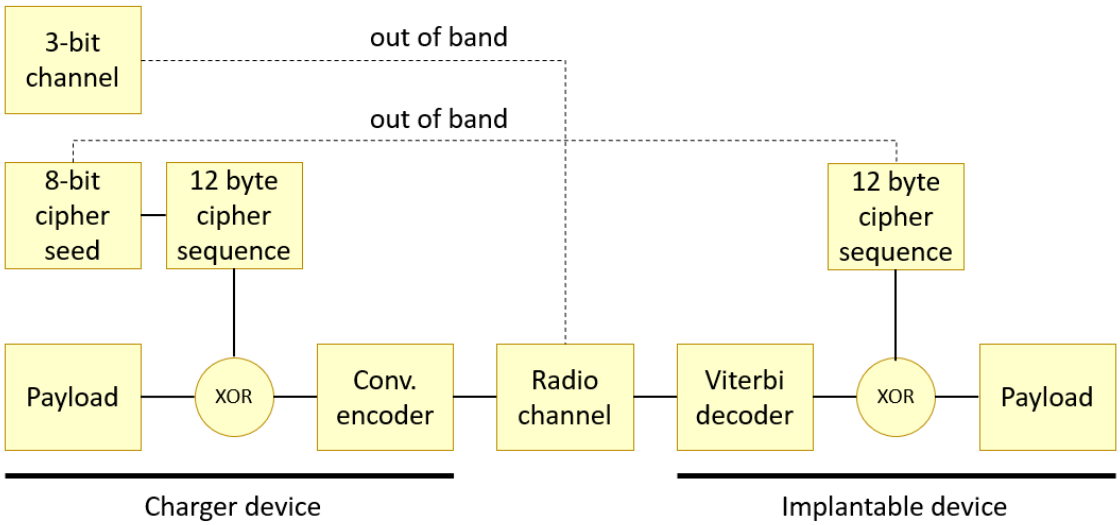

Figure 3: Logical scheme of the communication link

The complete structure of the communication channel is depicted in Fig. 3. This picture describes the communication process both ways. The 3-bit channel as well as the cipher seed are always generated on the side of charging device. This data is passed to the implantable device off-band using the H-field generated by the charging coil. The channel and cipher seed are the same for both uplink and downlink from and to the implantable device, respectively. First, the payload is encrypted by XORing it with 12-byte cipher sequence generated by the pseudorandom generator initialized with the 8-bit cipher seed. After that, the encrypted sequence is coded with a convolutional code and the resulting 24-byte payload is send through the channel to the receiver side where it is decoded using Viterbi decoder, XORed with the same pseudo-randomly generated sequence and the original payload is obtained.

13 Theory of magnetic field in wireless charging

13.1 Wireless charging requirements

The wireless charging in the device developed in this thesis is an inductive charging via very loosely coupled coils. The size of the first coil is fixed and is limited by the size of the enclosure of the implantable device. The motivation in the implantable device is to maximize the area of the coil to maximize the amount of magnetic flux going through the coil. The number of turns is also very limited and due to the overall small size, the number of turns was maximized so that the capacitor can be of C0G/NP0 dielectric due to very high temperature stability.

The only degree of freedom in the design of the coil lies in the charging coil. The expected working distance of the charger when the implant will be implanted is about 10 to 14 centimetres under the surface of the skin of the animal. The size of the wireless charging coil has to be reasonable due to its use case when the device will be. The maximum power draw from the 12 V rail is hardware limited to approx. 20 W (determined experimentally by measuring the temperature of power components) as the heatsink is not capable of dissipating more heat without active cooling.

13.2 Wire loop

To simplify the calculations, a wire loop will be taken as an approximation of the coil which is used. The magnetic field around the wire loop can be found using Biot-Savart law. This law is strictly used for static electric currents. For currents which change in time, retarded fields should be taken into consideration. However, the wire loop operates at a very small frequency (under 1 MHz) and the coil is not an antenna. Biot-Savart law cannot be used in antennas because it is defined as an integral over a closed curve. A simple dipole antenna with open end would thus violate the charge conservation law. In a coil, the current path can be closed within a curve. The Biot-Savart law is given by equation[22]:

$$\vec{B} = \frac{\mu_0 I}{4\pi} \oint \frac{d\vec{l} \times \vec{r_0}}{r^2}$$

Applied to the wire loop (= current loop) scenario, algebraic solution is possible. The B_x and B_y elements cancel each other due to symmetry and the only element of the magnetic field which is not zero is B_z.

$$dB_z = \frac{\mu_0 I dL}{4\pi} \frac{D}{(z^2 + D^2)^{\frac{3}{2}}}$$

Every element in dB_z is constant except for dL which is the circumference of the circle after integration of the curve integral. The magnetic field in axis of the wire loop in arbitrary distance from the centre can then be described as

$$B_z = \frac{\mu_0}{2} \frac{D^2 I}{(z^2 + D^2)^{\frac{3}{2}}}$$

The magnetic field around the coil respects the law of superposition so the magnetic field in axis of a compact N-turn coil can be approximated as:

$$B_z = \frac{\mu_0 N}{2} \frac{D^2 I}{(z^2 + D^2)^{\frac{3}{2}}}$$

where N is the number of turns. The inductance of N-turn coil can be approximated using this formula:

$$L_{coil} \approx N^2 \mu_0 \mu_r \frac{D}{2} \left[\ln \frac{8D}{d} - 2 \right]$$

Where N is number of turns, D is diameter of the coil and d is wire diameter.

From the formulas above, it is evident that the magnetic field is proportional to the current. Each coil has the impedance which consists of a resistance of wire and inductive reactance. Those two components are static (omitting temperature changes) and limit the amount of AC current flowing through the coil. There is a resonant circuit with the capacitor formed so the limiting factor is the capacitor rated voltage in the resonant circuit. The other limiting factor is the maximum current which can flow through the wires without significant heating of the coil which could damage the isolation of the wires and ultimately lead to destruction of the coil. To describe the situation fully, the impedance of the coil is:

$$X = 2\pi f L + R = 2\pi f N^2 \mu_0 \mu_r \frac{D}{2} \left[\ln \frac{8D}{d} - 2 \right] + \rho \pi D$$

Maximum current (omitting the resistance of the coil) at a given maximum voltage can then be described as:

$$I_L = \frac{U_{max}}{X} = \frac{U_{max}}{2\pi f N^2 \mu_0 \mu_r \frac{D}{2} \left[\ln \frac{8D}{d} - 2 \right] + \rho \pi D}$$

The magnetic field in a given distance z from the axis of the coil with diameter of R is:

$$B_z = \frac{\mu_0 N}{2} \frac{D^2 \frac{U_{max}}{2\pi f N^2 \mu_0 \mu_r \frac{D}{2} \left[\ln \frac{8D}{d} - 2 \right] + \rho \pi D}}{(z^2 + D^2)^{\frac{3}{2}}}$$

The analysis of this formula lead to a result without any local or global maxima (diameter going to 0 results in increasing of the current to infinity). This is of course caused by the increasing current through the coil. Although matematically correct, this situation is not possible in real-life scenario as from practical experience, the maximum current flowing through a piece of wire was determined using the AWG maximum current recommendation table[23]. The result is that for lower coil diameters, the current is the limiting factor while for larger coils, the limiting factor is the voltage across the capacitors. The maximum acceptable voltage across the capacitors was

determined to be 300 volts due to typical voltage ratings of EIA 3216 and EIA 4532 capacitors as well as the isolation distances on the PCB. This voltage is also equal to maximum peak to peak voltages on the inductor. A wire with cross section area of 1.25 mm^2 was used for coil in this design so the maximum urrent is 6.25 A RMS and the maximum voltage across the coil is 300 volts peak to peak (~ 106 V RMS).

At higher frequencies, skin effect also plays role as it effectively reduces the cross section area of the conductor. The skin depth formula is as follows:

$$\delta_s = \sqrt{\frac{1}{\pi f \mu \sigma}}$$

For f=750 kHz and copper material, the skin depth is 75 μm. To limit this effect, a stranded copper wire can be used. Instead of one solid piece of copper, multiple very thin strands are used to distribute the skin effect among all of them and increase the effective cross section area of the wire. By putting all the information together, the optimum coil diameter for the given range is 95 mm realized with stranded wire. The diameter was calculated by determining the maximum current for various diameters (either limited to 6.25 A RMS or limited by the maximum voltage). The skin effect was supressed by using stranded wire. On the printed circuit board, the thickness of the copper foil is 35 μm so the skin effect is supressed by design.

14 Electrical design of implantable device

Note: Schematic diagrams (Fig. 4 and Fig. 5) are provided at the end of this section

The absolute maximum size of the implantable device determined by a third party which will perform the implantation of the device into submucosa is about 30 x 15 x 6 mm. The minimum thickness of the plastic wall which can be reliably manufactured using the available instruments is 0.6 mm. The maximum PCB size, giving an overhead of 2 mm for hook for grasper and 0.2 mm of PCB clearance from each side of the enclosure, is 26.4 mm x 13.4 mm. Giving some additional overhead to unexpected changes in the mechanical enclosure design, the maximum size of the PCB was determined to be 25 mm x 13 mm. The printed circuit board is 4-layer to accommodate majority of analog and digital signals on top and bottom layer, while the power delivery network (ground planes and power planes) is contained in the inner layers. The minimum track width and track clearance is provided by the manufacturer and is 0.1 mm.

The electronics contains 6 main modules – battery charging circuit, power delivery circuit, step-up converter for stimulation circuitry, radio communication circuit, electrical stimulation signal generation circuitry and microcontroller. The first prototype of the electronics was populated by hand which put some constraints on the type of components which could be used. The BGA (ball-grid array) packages with ball pitch under 0.5 mm are practically not solderable manually without machine-assisted placement (either semi-automatic or automatic pick and place machine).

After manufacturing repeatability problems in previous prototypes of the implantable device, the charging coil was integrated on the printed circuit board. In previous prototypes, the coil was wound up by hand on a rectangular piece of plastic and glued together. After that, this coil assembly was glued on the printed circuit board. By measurement, the deviation of the inductance of 10 prototypes was over 10 % which affected the centre frequency of the LC resonant circuit on the implantable device. To limit this effect, integration of the charging coil on the printed circuit board was done to contribute to the overall repeatability of the resonant frequency which should be affected only by capacitor value deviation in the resonant circuit.

In previous prototypes, the coil was successfully realized with 18 turns of AWG42 wire and resonant capacity in terms of several nF with charging field frequency of 1 MHz. The number of turns of the coil increases the inductance which lowers the parallel capacitance which is desirable because of miniature construction. Lower capacitances are offered in smaller packages and also more temperature stable dielectrics (like C0G/NP0) are available. In this case the use of temperature stable dielectric is critical as the centre frequency of the resonant circuit would drift with small temperature changes. The coil is realized as planar on a printed circuit board which contains 4 layers. 16 turns with trace thickness of 0.1 mm and trace clearance of 0.1 mm were realized by putting 4 turns on each layer, while interconnecting the layers with vias. The clearance

from the edge of the PCB given by manufacturer is 0.3 mm. This means that the remaining space on the PCB for battery and electronics is 23.6 mm x 11.6 mm.

Next major step in the design of the implantable device was the choice of battery. From previous experiments, current draw exceeding 30 mA is required to facilitate the wireless communication and electrical neurostimulation. The battery should have sufficient capacity to power the implant for several days at least. The size of the battery is also a limiting factor as the length cannot be larger than 23.6 mm. Panasonic offers a portfolio of "pin-shaped" batteries based on Li-Ion chemistry. From this portfolio, only CG-320A[24] fits the size requirements of the implantable device. This type of battery was also successfully used in one of the previous type of implant and is proven to withstand in tissue for periods of time longer than 6 months. For safety reasons, the battery will be given 0.3 mm clearance from each side, resulting in 4 mm of PCB space occupied by the slot for the battery and additional 0.6 mm due to clearance requirement. Thus, the total space available for all electronics is 23.6 mm x 7 mm. While two side component mounting is possible, it is not favourable as it makes the manufacturing process significantly more challenging. In two-side component mounting, larger components usually must be glued to the PCB prior or after soldering to avoid falling off during the soldering of the other side, when these components will not be supported by gravity. Next, two-side component mounting will increase the thickness of the assembly. Given these arguments, single-side assembly will be preferred.

The previous prototypes were fitted with EIA0402 size passive components with modified (smaller) pad footprint and 0.5+ mm pitch QFN components. After some calculations and attempts in layout editor, this approach will not work in this case as the maximum occupiable PCB space is too small. Thus, a combination of 0.4 mm pitch QFN components, BGA components and most importantly, EIA0201 passive components will be used in the final prototype. A standard footprint for EIA0201 components in layout editor was used.

The microcontroller which was used in development of this prototype is from the same family as previous prototype – PIC16. Due to size constraints, PIC16F1718-E/MV[25] was chosen. The package size is 4 x 4 x 0.5 mm and it offers an extensive portfolio of digital and analog peripherals, including on-chip operational amplifiers, which reduces the overall footprint.

The power management circuitry can be divided into two main parts – battery charging and DC-DC step-down converter. The battery charging circuitry consists of a planar 4-layer PCB coil and parallel capacitor which forms the LC resonant circuit. Afterwards, using diode-capacitor doubler with Schottky diodes[26], the LC resonant circuit output signal is rectified and the voltage is doubled. The parallel resistor was used during development as a test-point to artificially inject voltage into the circuit to test its properties. It is also used to discharge the parallel capacitor when no charging signal is present. This is useful as OOK modulated signal from the charging device can be demodulated directly using a general-purpose input in the microcontroller. The OOK modulated signal is isolated from the battery with a series Schottky diode. In a normal state, the

charging process is controlled by a closed loop where the implantable device sends information about the battery voltage to the charging device which adjusts the power delivery. To make this system fail-safe, a simple protection with a 4.3 V Zener diode[27] was implemented. This protects the battery from overcharging as the current in case of closed loop battery charging control failure will flow through the Zener diode rather than charging the battery. Unused power will be dissipated as heat in the Zener diode. This represents a very simple charging circuit which is software-controlled rather than controlled by a wireless-charging controller IC. Specialized circuits were not used as the portfolios of chip manufacturers lack specialized solutions for wireless battery charging of both small capacity batteries and loosely coupled coils. For stable power rail generation, a single SiP (system in package) solution from Texas Instruments was used – TPS82740B[28]. It is a step-down converter with two outputs, while one of them can be controlled (switched on/off) by a logical output from the microcontroller. As a power saving feature, two operational modes are present. One of the DC-DC converters is running all the time (when sufficient battery voltage is present). This power rail which is constantly running, powers the microcontroller only. The microcontroller then controls the second power rail which powers the rest of the circuitry – the step-up DC-DC converter for neurostimulation and radio transceiver.

Current neurostimulators used in treatment of gastric disorders use stimulation voltages up to 12 V[8]. The implantable device in this thesis is designed to provide same stimulation parameters. Thus, the maximum stimulation voltage of 12 V is possible. The voltage is generated by MAX8570[29] step-up DC-DC converter in SOT23-6 package. The chip was connected in accordance with the instructions from datasheet, using recommended component values and properties.

NCS2004[30] operational amplifier in DFN package is used as a driver for neurostimulation. It is used as a non-inverting voltage amplifier with gain of +10. Its non-inverting input is driven directly by the microcontroller. This operation amplifier is unity gain stable according to datasheet so no additional components to compensate the instability were not required in the design. The output is connected to the pad on the back side of the PCB which is directly connected to the stimulation circuit on a flexible PCB.

Si4455[16] in QFN20 package is used as a radio transceiver to provide wireless communication capabilities to the device. It is powered from the switchable 2.7 V power rail. The shutdown pin is tied to GND as POR (power on reset) can be achieved by power cycling of the device. The ramp-up time of the power rail is under 300 μs (verified by measurement using an oscilloscope). The requirement of the chip is ramp-up time less than 1 ms for correct POR routine. The transceiver communicates with the microcontroller using 4-wire SPI bus. The matching network is realized with 0201 capacitors and inductors. 30 MHz crystal in miniature 1.6 x 1.2 mm packaging is used as a frequency reference. Tuneable parallel capacitor for crystal resonator is provided on-chip so no additional passive components are required.

To make the construction of the device easier and lower the thickness of the assembly, only the top side is populated. On the bottom side, 7 pads are provided for stimulation, programming interface and two-electrode amperometric sensor interface. The reason to is that the PCB is sealed after assembly. Thus, the programming access to allow for software modifications would be extremely limited. For the current goal of research, development of a bootloader would not make no sense due to its complexity. In future however, wireless bootloader with capability of software reprogramming would be a viable solution.

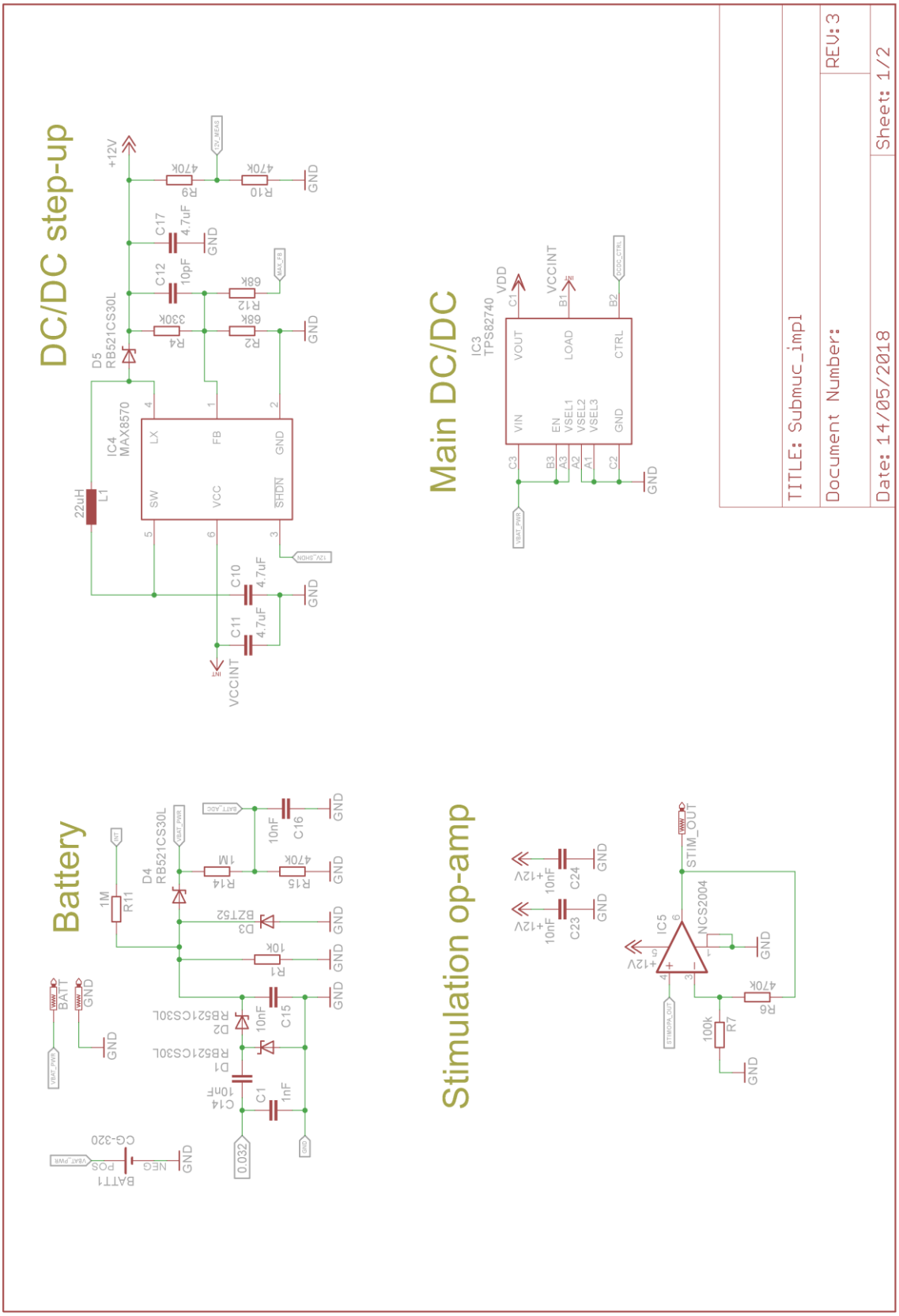

Figure 4: Implantable device circuit diagram - sheet A

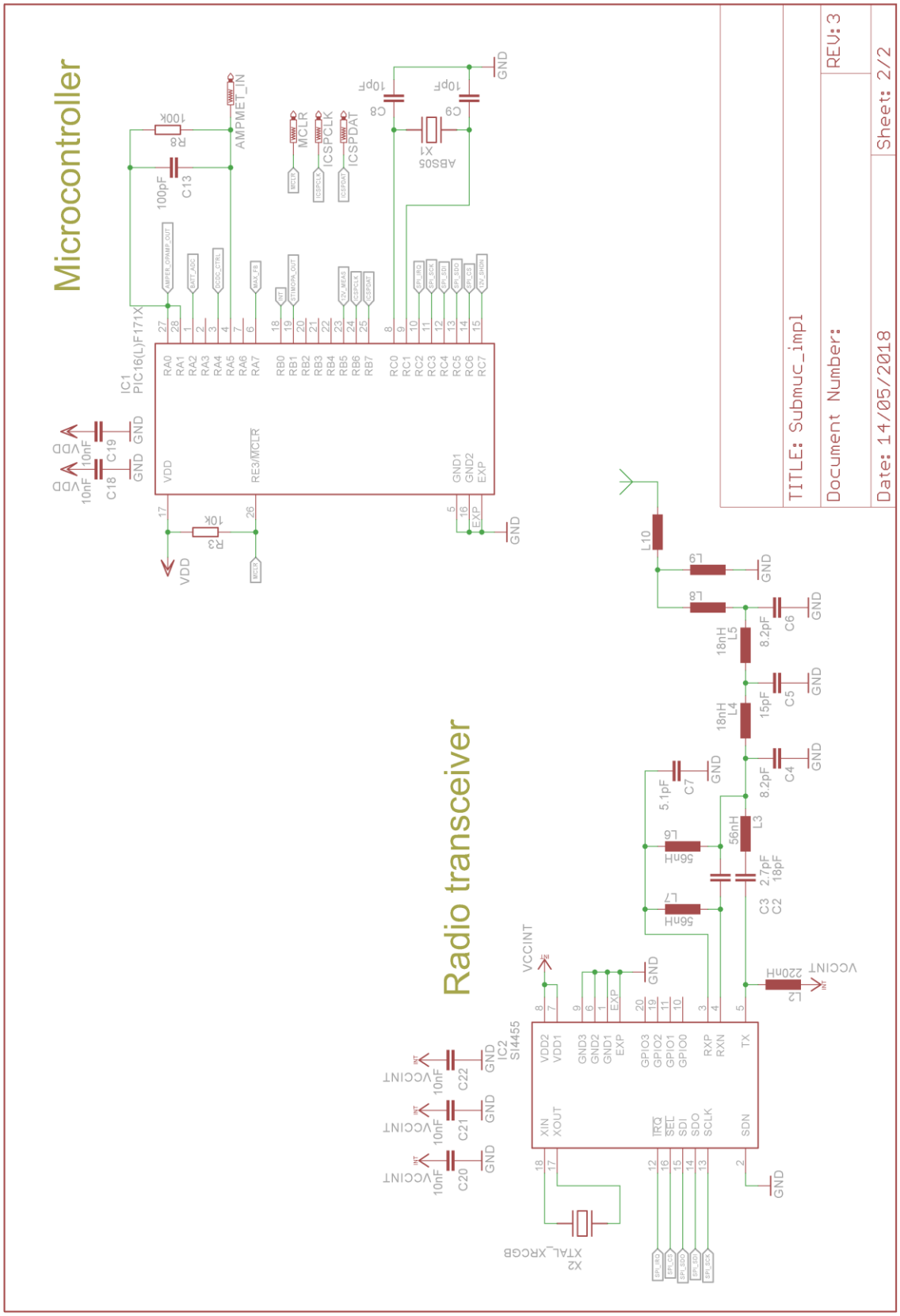

Figure 5: Implantable device circuit diagram - sheet B

15 Mechanical design of implantable device

15.1 Description of the enclosure

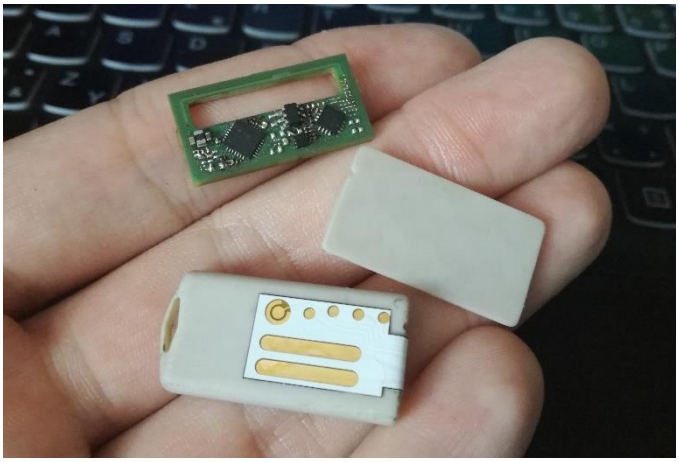

Figure 6: PEEK enclosure and PCB

Due to the nature of device implantation into submucosa, the device must withstand extreme surrounding conditions and mechanical stresses – from grasping the device in instruments used in endoscope to conditions when submerged in blood and other body fluids. The prototype needs to be at least partially sealed, if not hermetic. Next issue is the biocompatibility. The body's immune system will tend to reject the implant if it will not be manufactured from a material which is inert to the human body. Examples of such materials are titanium and glass. Those materials are proven to be effective and are extensively used in implantable devices ranging from RFID tags for animals to AIMDs like implantable defibrillators and pacemakers. Another advantage of titanium and glass is extremely low permittivity both to oxygen and moisture[31]. However, a great disadvantage is that working with those materials on a prototype level is particularly challenging. Thus, a polymer approach will be used during manufacturing of the enclosure for the prototype implantable device. High chemical resistance as well as resistance to sterilization is another factor which will be considered. The testing of polymers is usually done in vivo with ISO 10993[32] providing full guidelines to the testing scheme. There is one material which has been extensively studied and is used in implantable medical devices – PEEK (polyethylene ether ketone). It is used in trauma, spinal and orthopaedic implants. Other advantages are that it keeps tight tolerances during subtractive manufacturing (turning or milling). Is does not deform nor melts easily during machining operations.

The enclosure for the implantable device comprises of two PEEK elements which are glued together with an adhesive which provides good sealing properties over the duration of typical experiment (48 hours for model and non-survival procedures, 2 weeks for a short survival experiment). A small gap is manufactured in the side of the enclosure to allow the flexible PCB with stimulating electrodes to be placed outside of the main enclosure. This way, the electronics is fully protected while the programming interface and direct battery contact for charging is still provided for development purposes.

15.2 Manufacturing of the enclosure

The enclosure itself was machined using a small 3-axis CNC machine with 800 W water-cooled spindle and mist cooling. Mist cooling was enabled during the machining to reduce the temperature of the machined surface and reduce deformation and burr formation. A special holder for the PEEK material (Fig. 8) was developed to facilitate fast production of the enclosures. A pre-cut piece of PEEK material fits inside the holder with very low clearances and is held in place using two or four M3 screws. Each program has two operations – one from one side and second operation from the other. The 3D model was developed in Autodesk Fusion 360 software which also includes CAM package for generation of G-code for the machine. This G-code is then transferred to the computer which operates the machine. A combination of 1 mm and 2 mm HSS (high-speed steel) flat end mills was used to machine the enclosure.

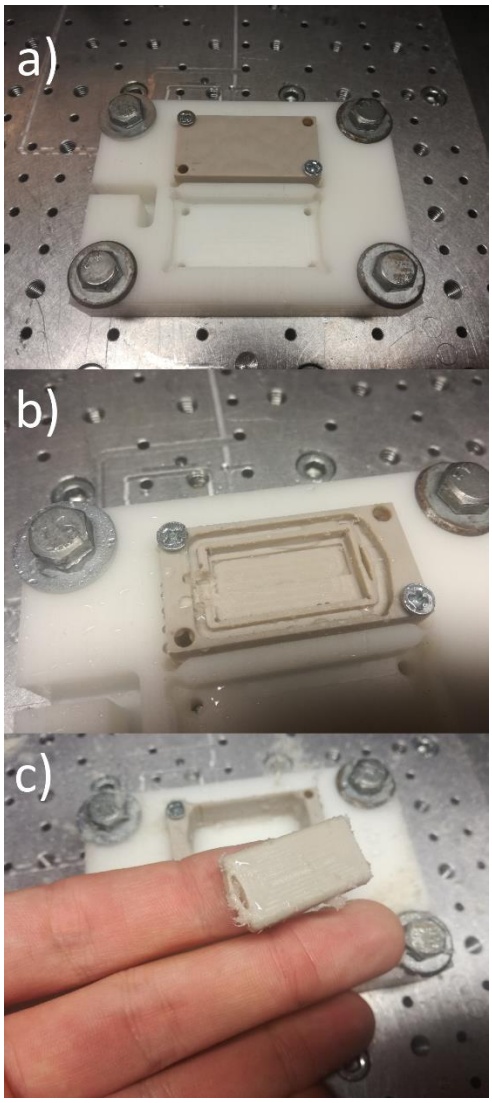

Figure 7: Fixture and PEEK material

First, the fixture for PEEK blocks was manufactured. The purpose of the fixture is to hold the PEEK material during the machining and to allow easy rotation of the piece during the second machining operation. After that, the PEEK block was machined and put into the fixture and fixed by two M3 screws (Fig. 7a). Then, the first operation was done to mill the inner cavity for the electronics and battery (Fig. 7b). After that, the PEEK block was turned over, fixed by two screws again and the second operation which worked out the back side of the implantable device was completed, and the piece was cut out (Fig. 7c). The second PEEK part was easier to manufacture as it was manufactured in a single operation only (the back side is flat). Both parts were manually deburred and cleaned with distilled water and 99 % isopropanol.

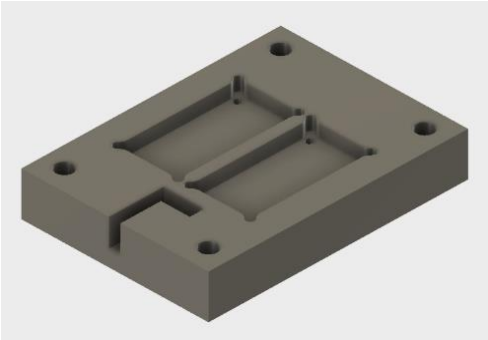

Figure 8: Fixture for PEEK blocks

16 Design of the charging device

Note: Schematic diagrams (Fig. 11 and Fig. 12) are provided at the end of this section

16.1 Electronics

The charging device is designed as a single 4-layer PCB. Unlike the implantable device, it is powered from USB and external 12 V power adapter. 5 V USB power is used for low-voltage logic (USB <-> UART converter, microcontroller, display, RF transceiver) while the external 12 V power adapter is used to power the wireless charging circuitry. A resettable fuse is provided both at 5 V (0.5 A threshold current) and 12 V (5 A threshold current) power rail. The 3.3 V power rail for microcontroller, RF transceiver and display is created with a LD1117[33] 3.3 V low-drop linear regulator in SOT223 package. FT232RL[34] transceiver is used to create a virtual COM port on the PC where the device is connected to. It converts between USB bus and 3.3 V UART. PIC16LF1783[35] is used as the microcontroller. It communicates via SPI bus with both ST7735-based TFT display and Si4455[16] transceiver. The circuit diagram of Si4455 transceiver is same as for the implantable device, the only change is that 0402 passive components are used and UFL type connector is used for connecting of the antenna.

Figure 9: Charger device with display

The PSMC module of the microcontroller is used for generating of the PWM signals for MOSFET full-bridge which drives the LC resonant circuit of the charging coil. The four PWM signals which drive the full bridge are connected to two NCP5183[36] half-bridge bootstrap MOSFET drivers. NTMFFS[37] series N-MOS transistors are used to drive the LC resonant circuit. The resonant circuit comprises of an inductor and parallel capacitor bank which is tuned to the charging frequency to maximize the current flowing through the coil. This current induces oscillating magnetic field which is propagated to the receiver coil in the implantable device. All low-voltage components except for 12 V power rail input and filtration capacitors are in the lower portion of the printed circuit board. All power electronics (MOSFET drivers and MOSFETs themselves) are placed in the top side of the PCB. As the power components have non-uniform height and emit a lot of heat, 2 mm flexible and compressible thermal compound[38] was used to establish a sufficient thermal contact between the components and custom CNC machined aluminium heatsink to dissipate the heat generated by the components. The use of thermal compound eliminated the

need to machine a rather complex shape of the components populated on the PCB and avoided additional mechanical stress to the components caused by irregularities of either assembly or aluminium heatsink. The aluminium heatsink itself has four threaded holes which are used to screw it to the bottom plastic assembly. This also fixes the PCB to the bottom plastic assembly. The top plastic assembly is screwed to the bottom assembly which finalizes the main body. To protect the charging coil, a special enclosure was designed and manufactured. The enclosure comprises of two plastic parts which are put together by one screw at the top and two screws in the bottom part which are also used to screw the coil to the bottom part of the main enclosure. Both 12 V power adapter and USB cable are soldered to the board and provided with strain relief rubber pieces at the edge of the enclosure.

16.2 Enclosure

Figure 10: Plastic enclosure for the lower portion of charger device

The enclosure for the charging device was milled in a similar way as for the implantable device. However, black Delrin material was used as biocompatibility is not a primary parameter in the charging device. The charging device will be outside of the body of all times and will not be in contact with any tissue except for hands of the person operating the device. The enclosure can be divided into two main parts – the main body which contains the electronics as well as the 400 MHz antenna and the coil body which contains the charging coil and protects it from outside environment against damage. The printed circuit board is divided into two distinct parts – the lower parts which contains the logic electronics, display and buttons and top part which contains the power electronics for charging. The power electronics – specifically the MOSFETs and drivers - generate a considerable amount of heat due to energy dissipated during switching. The amount of heat which is generated cannot be dissipated through the PCB without airflow. Thus, a custom aluminium heatsink was designed and milled from a block of aluminium. The height of the MOSFETs and drivers is not equal. Also, there are other components higher than the cooled components. To avoid designing complex enclosure and possibly generate stress or cause short circuit to the enclosure, a different approach was chosen. A special thermal conductive compound which is not electrically conductive and is stretchable and compressible was inserted between the cooled parts and heatsink. This also assures that other components which might get hot from the other components, are cooled and the whole electronics

is kept at a constant temperature. The heatsink has two M4 tapped holes on sides. These holes are used to fix the printed circuit board as well as the heatsink to the bottom part of the main part of the enclosure. Both cables – USB and +12 V power rail are soldered directly the board to avoid unwanted disconnecting of the cables during the experiments. Both cables are equipped with means to avoid ripping them off the board by accident.

The coil assembly is screwed to the top part of the main body of the enclosure. It consists of two pieces – the lower piece with a wide groove to accommodate the wire loops forming the main charging coil. The top piece screwed to the top main body piece with two screws and one plastic screw to the bottom coil piece protects the wire coil from damage.

There are total of two sets of wires coming out of the device – a USB-A cable, 3-meter-long as well as 4-meter-long +12 V rail cable which is connected to the 110-230 VAC adapter. The whole assembly is designed to be powered from two SELV/battery power supplies (PC/laptop and 12 V adapter) operating at DC supply voltages under or equal to 12 V.

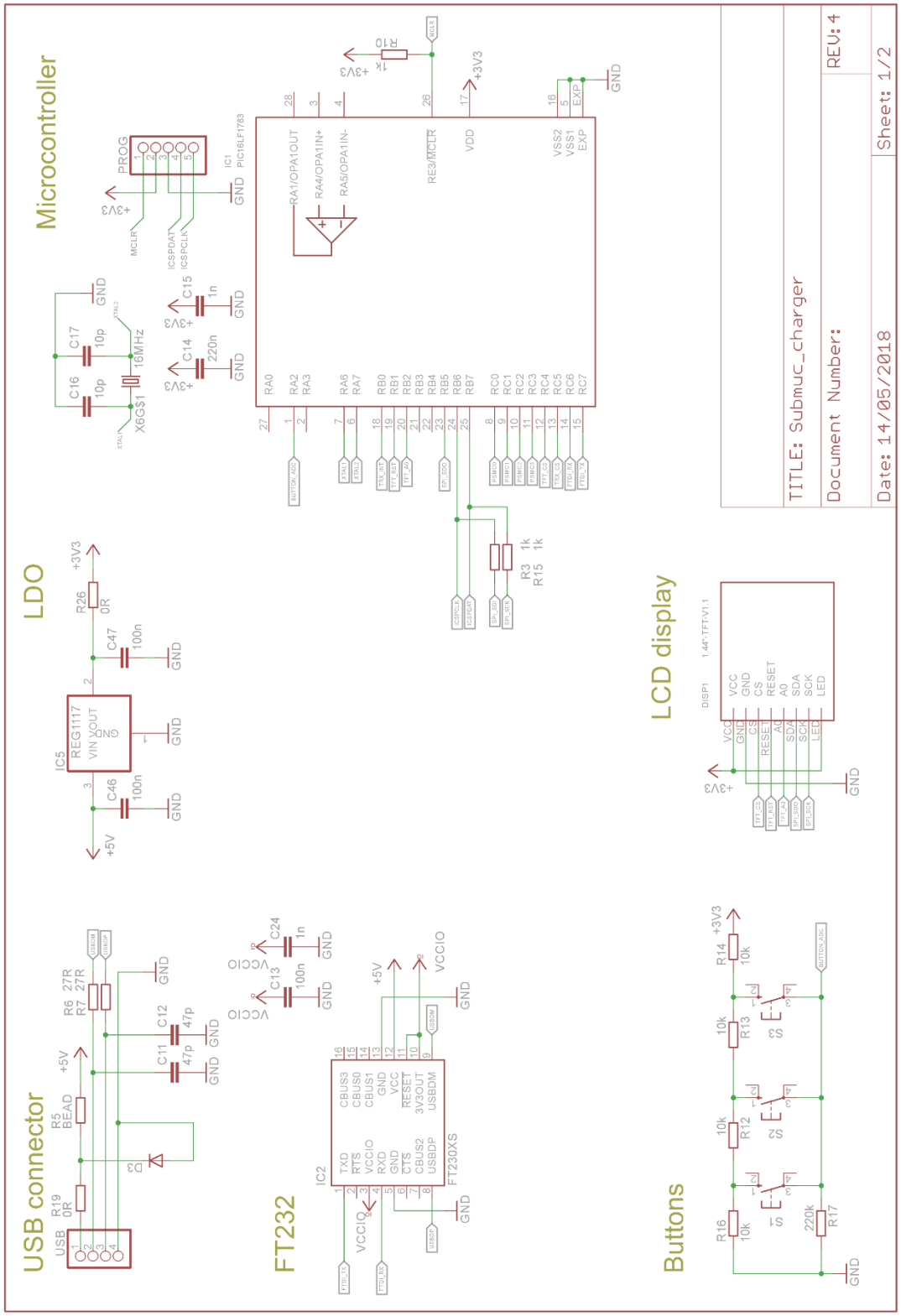

Figure 11: Charger device circuit diagram - sheet A

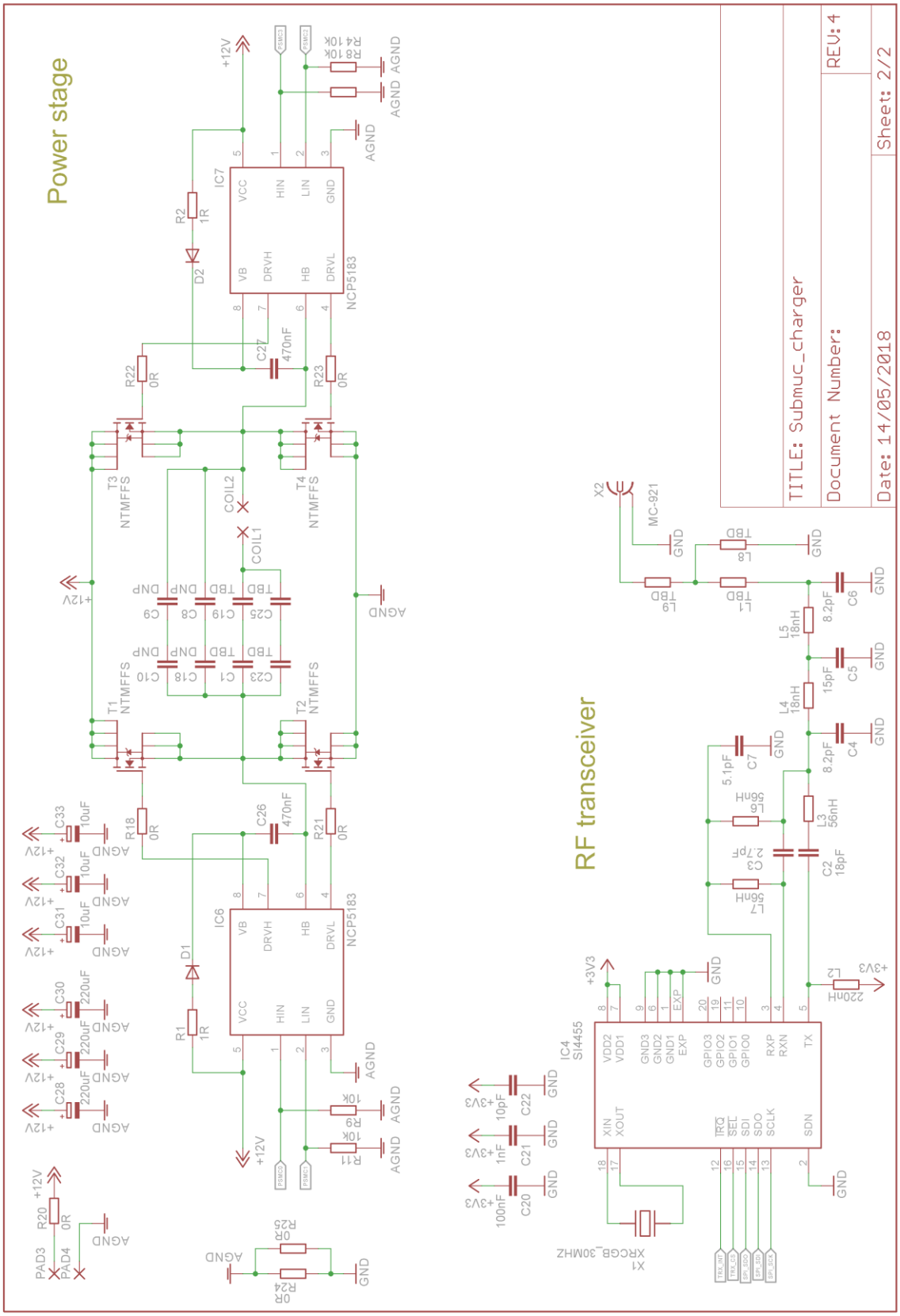

Figure 12: Charger device circuit diagram - sheet B

17 Software

17.1 Design tools

In the design of the implantable device charging device, two very similar PIC16 microcontrollers were used. For programming of the firmware for the microcontrollers, the MPLAB X IDE, Code Composer plug-in and PSMC Designer were used. The code was written in C programming language.

17.2 Implantable device

To avoid errors in setup of peripherals during the development, the Code Composer plug-in in the MPLAB X IDE together with the datasheet of the microcontroller. Except for GPIO, total of 6 peripherals in the microcontroller were used. The GPIOs were setup according to the circuit diagram and the expected functions of the device. The RA4 pin is set as an output to control the switchable power rail in the DC-DC converter. Next, the RC2 pin is configured as an interrupt-on-change pin because it is connected to the external interrupt of the Si4455 radio transceiver. Finally, the RC7 pin is connected to the shutdown pin of the MAX8570[29] step-up DC-DC converter. The oscillator is set to internal oscillator block with frequency of 4 MHz. The watchdog timer is enabled with WDT postscaler set to 1:32768 so it needs to be cleared approximately once every second. The reason the period is only approximate is because the internal oscillator reference used for WDT is on-chip and is very not precise (LFINTOSC).

Both on-chip op-amps are enabled. The OPA1 which is used for two-electrode amperometric measurement is set to *Low_GBWP* mode as the amperometric enzyme-based measurements are usually slow. On the other hand, the OPA2 which is used for generating of stimulation pulses which are often only a few tens of microseconds long, the GBWP is a limiting factor in terms of speed of rise and fall edges. The OPA2 is used as a buffer for the DAC (digital-to-analog converter) inside the microcontroller and is set to *High_GBWP* mode for this reason. Next peripheral is the FVR which generates 1.024 V reference to analog circuitry. This reference is then amplified by a factor of +2 and provided to DAC and ADC (analog-to-digital converter). The analog temperature sensor is a part of FVR peripheral and is enabled as well. TMR1 timer is enabled and set to a period of 100 ms (exactly 100.0977 ms). This is the base period for stimulation cycles. The stimulation cycles on and off cycles are provided in multiples of these periods. This timer also resets the WDT timer together with the program running in main cycle (both program in main cycle and WDT timer must confirm that they are running before the WDT is reset. The ADC module is configured to a sampling frequency 87 kHz which represents a TAD (acquisition time) of 1.0 us. The ADC is a SAR ADC which requires 11.5 TAD to perform a 12-bit AD conversion. The positive reference is FVR while the negative reference is VSS. During the power rail voltage measurement, the positive reference is switched to VDD and the FVR

voltage is measured (there is a dedicated FVR channel in the microcontroller). The external interrupt (RB0) is connected to the rectified voltage on the coil which passed the diode doubler. The signal is fed into the RB0 pin through 1 $M\Omega$ series resistor (to limit the current into the pin). The interrupt is generated if there is a high-to-low transition at the pin (the charger sends a logical 0 via OOK modulated charging magnetic field). The last peripheral which is used is the MSSP peripheral which is configured as a SPI Master. The SPI mode is set to 0 according to the Si4455 datasheet[16] which is the only SPI peripheral in the implantable device. This means that the clock polarity is set so idle state of clock line is logical low and active state is logical high. The clock edge, active to idle in this case, defines when the data change occurs.

The program is divided into two cycles – routine which runs in main cycle and routine which occurs during the TMR1 timer overflow. After power-up, initialization of all peripheral as well as the initialization and test of the Si4455 radio transceiver is performed. The initialization and operation of the radio transceiver is performed both in implantable device and charging device so a separate chapter is dedicated to it. Prior to initialization of the radio transceiver, the controllable DC-DC converter power rail was turned on by setting the appropriate output. After that, all unused peripherals are disabled to save power (including the controllable power rail) and the microcontroller is put to sleep mode to reduce the power consumption to minimum. When a high-to-low interrupt occurs at the GPIO, the interrupt routine is activated. The program waits for a pre-determined period – 115 ms (100 ms + 15 ms till the middle of the bit) to receive a logical 1. If logical 1 was received, there is wireless communication request. After that, the program reads total of 12 bits (every 30 ms) and checks the parity bit. If the parity check fails, the interrupt routine ends. If the parity check is correct, the transceiver in the implantable device is set into receiving mode and it awaits a packet from the charging device. The channel number is set based on the OOK modulated received message from the device. The decrypting and decoding of the message is based on the algorithm described in chapters 10 and 11. The parameters of neurostimulation are saved into RAM of the microcontroller and reply in the same channel is transmitted at least 10 ms (to allow time for receiving device to reconfigure into receiving mode). The reply serves as an acknowledge packet as well as a way to transmit telemetry data. The packet structure is described in full in section 10. During normal operation when there is no charging present, the microcontrollers is in sleep mode most of the time. The LFINTOSC oscillator is running and toggles the interrupt event every 100 ms. 100 ms was chosen as it is a minimum on and off-state stimulation state increment. The on and off-state intervals are saved in an uin32_t variable within the program. Each of those can be set to value from 0 to 6048000 which represents intervals from zero to 1 week (in 100 ms units). The value inside of the timer interrupt is incremented until it reaches the off-state value. Then, the stimulation starts by starting the stimulation timer. The stimulation itself is operating in stimulation timer interrupt operated from the main oscillator which is on during the stimulation event. The frequency of interrupt is set to

the actual stimulation pulse frequency. Within the stimulation timer interrupt, the DA converter is set and reset with a DAC value calculated from the desired stimulation voltage. The corresponding DAC values to stimulation voltage as well the stimulation pulse intervals as the stimulation are located in look-up tables in ROM.

17.3 Si4455 radio transceiver initialization and operation

The Si4455 Sub-GHz radio transceiver[16] was chosen because of low PCB footprint (a chip larger than 3x3 mm would not fit on the board) as well as the capability to communicate in the 402 MHz band. The initialization of the chip is done in two steps – the first step is to reprogram the transceiver with a "patch" provided by a chip vendor. This patch is composed of 512 bytes of data which are transmitted via SPI in 64 transmissions (8 bytes each). Before starting the next transmission, the CTS (clear to send) flag is checked. This is done using a special function (*si4455_check_CTS*) which continuously checks for the CTS until it is cleared. For safety reasons, the maximum number of repetitions is limited to 5000 to avoid freezing the microcontroller. A transmission which consists of 0x44 byte transmitted to the transceiver and reading the next byte is used. If the byte which is read is 0xFF, the chip is cleared to receive next data. If not, the cycle continues until the chip is ready. After the patch is applied, normal initialization procedure follows. The complete initialization sequence must be generated using a specialized software *WDS3* provided by Silicon Labs. This software generates arrays of initialization code as well as universal library for communicating with the chip which can be ported to any microcontroller family. This library was ported to MPLAB X environment and the SPI libraries for handling the communication were written in C. The chip has both hardware and software interrupts. After initialization of the radio, the microcontroller monitors these interrupts and waits for *PACKET_RX_PEND* if waiting for receipt of a packet or *PACKET_TX_PEND* to wait until the transmission of the packet was finished.

The transmit of the packet is initiated by writing the payload into the FIFO. After that, the *START_TX* state is by sending a SPI packet with an 0x31 command followed by 4 parameters, defining the channel and length of the packet which will be transferred. After that, the *PACKET_SEND_PEND* interrupt is polled until it is set. After that, the packet transmission was completed. The procedure for receiving a packet is similar, the difference is that after the RX mode start (by flushing the FIFO and initiating the RX mode with 0x32 command) the program waits until *PACKET_RX_PEND* interrupt is issued. After that, the FIFO is read out. As the packet length is known and does not change, 24 bytes (12 bytes coded by ½ convolutional code) are read out from the FIFO. Both transmitted and received packets are encoded and decoded including encryption and decryption using the functions described in chapter 10 and 11.

17.4 Charging device firmware

The code for initialization of the peripheral was generated by the Code Configurator plug-in similarly as in the implantable device. Additionally, PSMC software tool by Microchip was used to configure the PSMC module. The PSMC module is used for driving of the MOSFET full bridge which drives the series resonant LC circuit. The MSSP module is set to SPI master. There are two peripherals which are controlled with the SPI bus – Si4455 transceiver and ST7735 240 x 128 px color TFT display. Each of those peripherals has its own chip select output from the microcontroller. Ona analog input is used for buttons. As the charging device is the master (initiates and ends) in the wireless communication with the implant, the program is running in main cycle only, without timers and other interrupts which could introduce unwanted timing errors. At the beginning of program, all peripherals are initialized including the Si4455 radio transceiver and display. Next, in the while cycle within the main procedure, the buttons are continuously monitored. Also, the RSSI in all 8 channels is monitored and RSSI values are written on the screen in real-time. The first button toggles the H field – charging of the implantable device. The second button is used to set the stimulation parameters – long press of the button switches between the parameters while long shorts increment the value. The third button initiates the transmission – short press retrieves telemetry information only while long press transmits the stimulation parameters and retrieves telemetry from the implantable device.

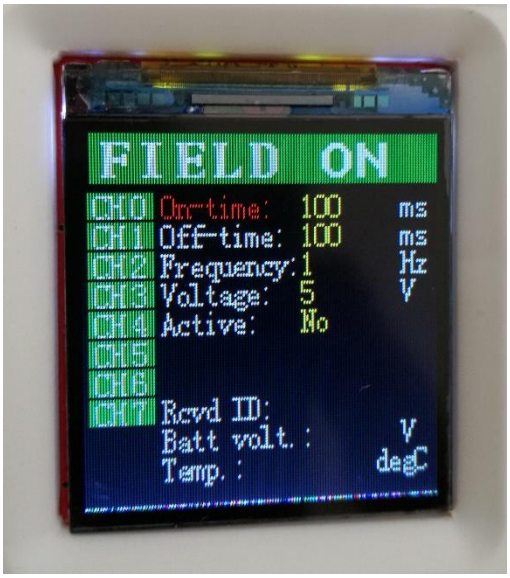

Figure 14: Charging device GUI

The display is used to show the important data to the user (Fig. 13) – namely the status of charging field, real-time channel occupation (prepared for further research), configuration parameters and the received data from the implantable device. The device is operated using 3 buttons located above the display. The location of the buttons was located so the device can be comfortably operated with a single hand (Fig. 14).


Figure 13: Charging device ergonomics

18 Manufacturing of the devices

18.1 Implantable device

The electronics was realized on a 1.6 mm thick 4-layer PCB with ENIG (electroless nickel immersion gold) surface finish. ENIG surface finish was preferred because of its flatness. When the PCB is immersion tin plated, surface irregularities make component placement harder, from author's experience especially when the components are smaller than EIA 0603 size. The components on the PCB were hand-placed and hand-soldered using an airflow gun. Lead-free no-clean Sn/Ag/Cu solder paste from Chip Quik company was used for SMT components larger than EIA0201. Those components were soldered first by dispensing the paste manually with needle dispenser on the pads, placing the components using tweezers and manual hot-air reflow. The temperature of the board and components was monitored by placing a Type K thermocouple on the board with a piece of Kapton tape. Special care was given so that the temperature of the components and board did not exceed 260°C to avoid damage of the components. For EIA0201 components, a different approach was chosen. Manual dispensing of the solder paste is almost impossible due to overall tiny size of pads. Also, with smaller diameter of the needle, the pressure to expel the paste from the needle tip increases. Pressure of 7 bar which is a maximum operating maximum pressure for the valves inside of the dispenser was not enough to pass the solder paste through 0.25 mm input diameter needle. Thus, normal lead solder (Sn62 Pb38) was spread manually using a soldering tip on 0201 pads. After that, the pads were cleaned of the flux. Next, a thin layer of *Stannol* brand contact soldering paste was spread over the pads and components were placed. Finally, the board was very carefully reflowed to avoid component movement. After soldering, the board was checked under the microscope for potential short and open circuits. Where possible (for example the resistor divider of the step-up converter), continuity of the circuit was checked using a multimeter. The last step was checking the continuity of the wireless charging coil. In 1 out of 5 boards which were soldered, the charging coil continuity was compromised, probably during the final grinding of the edges of the board before soldering.

Next, 5 enamel coated wires – 2 for power supply and 3 for programming were soldered to the back side of the board to test each board before putting and gluing it into the enclosure. The test program was uploaded into the device and measurements were done. First, the test program switches the step-up converter off and on both set to 6 V and 12 V output voltage. Then, the output of the stimulation op-amp is swept with triangle waveform from 0 V to 12 V and back to 0 V. Radio transceiver is set to continuous TX mode and the RF power at 402.15 MHz is measured with TrxEB evaluation board with CC110L 433 MHz module with external antenna. After that, final firmware was downloaded to the microcontroller, wires were de-soldered, pads were cleaned of any remaining solder with soldering wick and the board was cleaned thoroughly in 99% isopropylalcohol and dried at 60°C for 30 minutes in a temperature-controlled oven. After that,

3M 9703 Z-axis anisotropic conductive tape was used to attach the flex cable to the PCB. The tape was bonded to the materials by pressure generated by a finger. The recommended minimum overlap area is bigger than the area of the pads, but several experiments were done, and the overlap is sufficient, and no problems were detected so far. In future, another type of anisotropic adhesive from 3M – 3M 7303 - which is bonded at elevated temperatures (140°C) and higher pressure (up to 2 MPa) will be used to achieve more reliable contact.

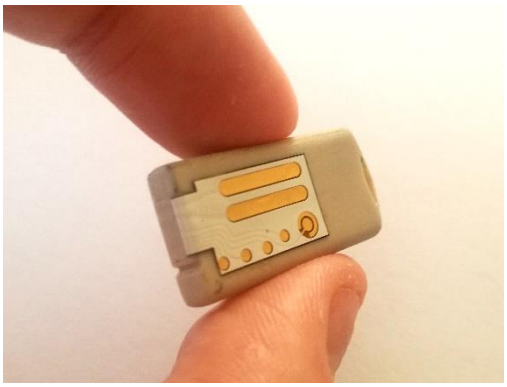

Figure 15: Finalized implantable device prototype

After bonding and testing of continuity of traces with multimeter, the battery is soldered to the contacts on back side of the board. The functionality of the wireless charging is tested with the wireless charger unit. If the battery voltage increases when the charging coil is given to the proximity of the device, the battery test is done, and the device can be fully enclosed. The board is inserted into the bottom part of PEEK enclosure and fixed with small amount of epoxy glue. After that, epoxy glue is applied to the edges of the enclosure as well as to the edge of the flex cable with the enclosure and the top lid is put on and pressed with 500 g weight to properly seal the enclosure. After 24 hours, the glue is completely set, and the functionality of the device is tested. If it passes this test, the next step is to glue the flexible portion on the back side of the enclosure. This is done with the same type of glue as the adhesive used for the enclosure. The last step is the isolation of the programming pins. This was done with 10 % solution of PMMA polymer in dichloromethane solvent. 1 μl of the solution was micropipetted on top of each gold plated pad and let to dry. After that, the device manufacturing is completed and after another 24 hours to wait for the glue to set. The final testing is done in 50 cm high column of physiological solution (0.9 g of NaCl in 1 litre of water).

18.2 Charging device

Similarly to the implantable device, the electronics was realized on a 1.6 mm 4-layer PCB. All components are larger than EIA 0402 so a lead-free soldering paste was used to solder all components to the board. After soldering with a hot air gun, the board was visually tested and the programming device was connected to the board to

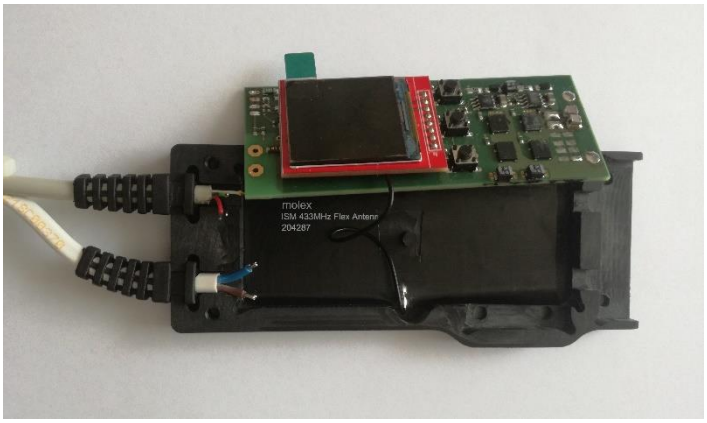

Figure 16: Assembling the PCB into charger device

program the test firmware to the microcontroller. The functionality of the PSMC module was tested with a 4-channel oscilloscope viewing all PWM signals. Radio transceiver was tested in an analogous way as in the implantable device – by configuring it and transmitting a continuous carrier at 402.15 MHz. After that, the display is tested – first by pressing the metal pins against the holes with vias in the board. If the display correctly initializes after reset of the microcontroller, the button test is executed. If it passes, the test of the digital circuitry is completed, and the display is soldered directly to the board.

Figure 17: Finalized charger device

After that, cables with rubber strain reliefers are inserted into the bottom part of the enclosure and soldered to the board which is also placed in the enclosure. Before the final placement of the PCB, the antenna is placed on the bottom of the enclosure. The top coil is placed onto the top part of the enclosure, the wires are soldered, and the top coil cover is placed over the coil. Then, the middle spacer and the white top part of the enclosure is placed over the electronics and fixed with four M4 x 15 screws. Then, the heat conductive pad is cut out and placed on the power components. Finally, the aluminium heatsink is placed on top and fixed with 4 screws on the opposite side. The coil cover is glued to the main coil body.

19 Endoscopic implantation to submucosa

The implantability of the device into submucosa was practically tested during an endoscopic training session in Fakultní nemocnice Královské Vinohrady. A pig stomach with esophagus was used with the Olympus Evis Exera II endoscope dedicated for animal use only. The implantation was done by MUDr. Jan Hajer, Ph.D. The process of implantation of the device into submucosa is depicted on Fig 18.

First, the device was inserted to the stomach via pylorus. A pocket in the submucosa was created in a few steps. First, the submucosa where the device would be implanted was injected with a physiological solution of methylene blue. The purpose of the methylene blue is to highlight the submucosa. The submucosa is a gel-like irregular connective tissue or loose connective tissue. Unlike muscle, the methylene blue solution colours the submucosa. After that, an incision was made with an endoscopic dual knife through the mucosal layer into submucosa. After that, the submucosa was dilated and cut (Fig. 18a) with the endoscopic knife to form a pocket large enough to facilitate the implantable device.

After that, the endoscope was inserted to the esophagus without the cap. A grasper tool was used to manipulate the implantable device inside the submucosa (Fig. 18b). Then, the device was directed (Fig. 18c) and placed (Fig. 18d) into the submucosal pocket. The correct position (electrodes have direct contact with the muscular tissue (Fig. 18e) was checked and finally, the device was secured in the submucosal pocket with two haemostatic clips which close the wound (Fig. 18f).

The implantation was successful and can be performed by an endoscopist experienced in submucosal dissections in under 20 minutes. Multiple mechanical features are present on the device to make the process of implantation easier. First, the device itself is manufactured to have as few sharp corners as possible to avoid traumatization of the tissue and make the insertion to the submucosal pocket as easy as possible. Next, the device is equipped with two means to attach the implantable device to the instrument. The first means are two grooves at the shorter sides where a disposable snare can be used to catch the device and transfer it into submucosal pocket. Secondly, a hole is created on one side, so a single use grasper may be used for the implantation. Also, the electrodes have a distinctive color and appearance so the endoscopist may orient the implantable device easily. The PEEK material as well as gold plated electrodes and polyimide flexible base material are resistant to hydrochloric acid, so it can be placed in stomach for an extended period of time during implantation.

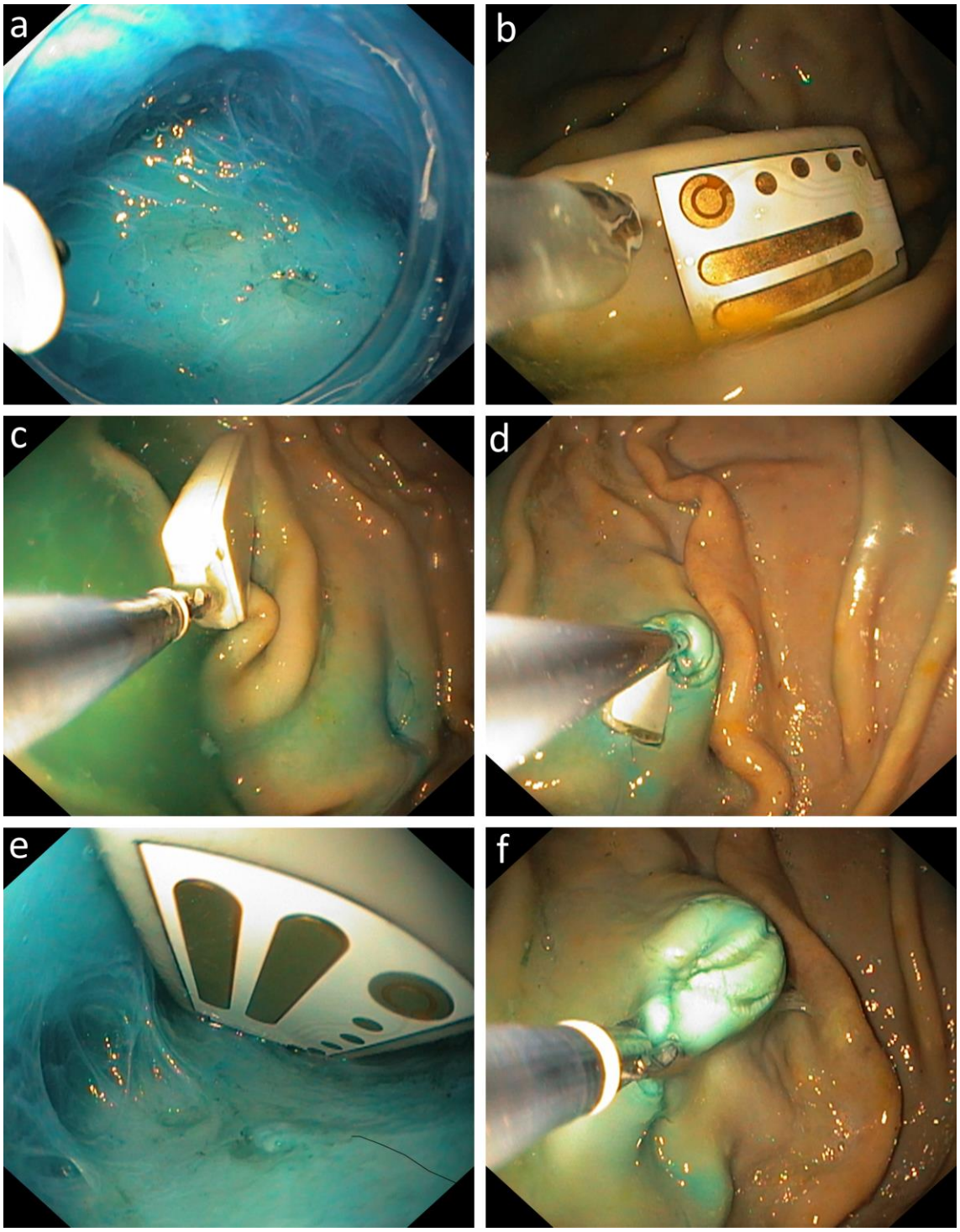

Figure 18: Implantation of the device into submucosa

20 Discussion

The implantation of medical devices into intramural space – submucosa – is a very perspective area for research in the upcoming years and decades. As stated in the beginning, this space is virtual and has to be created artificially, most preferably with an endoscope. Currently the endoscopic techniques which are working in or near submucosa focus on resection of tumours. However, in last few years, increasing attention is given to implantable devices which could be implanted to submucosa.

The major limiting factor of implantable devices in the submucosa is the limited battery storage. Current implantable devices are placed subcutaneously due to their large sizes because of internal battery which is non-rechargeable. Miniature wire electrodes are inserted into the muscle tissue from the outside. Implantable devices inserted from the inside offer a huge advantage in both patient comfort and device safety. A simple wireless charging system was developed to achieve sufficient electrical energy supply during the up to several-week long test trials on living pigs which will follow. Compared to previous research done on this subject, this implementation of an experimental implantable device in submucosa offers a superior advantage in combining embedded energy storage for high current energy spikes which may occur during high-voltage neurostimulation and possibility to wirelessly recharge the battery in order to significantly prolong the battery life. At the same time, the battery can be extremely small which makes the overall dimensions of the device very small.

The major technological challenge in design of implantable devices is the design of wireless communication link. The communication link has to be reliable as well as low-power. The choice of the suitable frequency bands is pre-defined by regulations. Even at those very low frequencies (in 400 MHz) band, the attenuation caused by the human body is notable, if not significant – about 20 dB. The choice of such low frequency means that the antenna has to be electrically small at least at the side of the implantable device. In the presented solution, the maximum permissible length of the antenna is less than 1/20 of the wavelength which causes extremely low radiating efficiency. However, electrically small antennas have very low directivity which is favourable as the angular position of the implant is not significant (for wireless communication – to effectively charge the battery the angular position of the coils is significant). Improving the gain of the antenna was not a primary goal of this thesis. It is one of the challenges which will have to be addressed in the future to make the communication more reliable. Also, the biocompatibility and choice of the materials will have to be completed to make the device completely safe for long-term animal trials.

21 Conclusions

The main goal of this thesis was the development of a system which could be used in research of submucosal implants. Particular focus was given to the design and implementation of wireless communication system. A complete system comprising of several layers which covers packet parsing, encryption and channel coding for secure and safe communication was developed. A unique system which consists of 400 MHz radio link with out-of-band transmitted secret key for encryption was successfully designed, implemented and tested.

One of the most limiting factors of development and testing of these systems in research is the size of the implant and cost. The presented solution represents a balance between very low manufacturing costs and size. Further miniaturization could be achieved by using BGA or CSP (chip-scale package) components or by integration of the electronics into a single ASIC (application-specific integrated circuit). This would however extremely increase the cost for prototyping and such modifications make sense only in actual development of device intended to be used in pre-clinical stage or on human subjects. The total BOM (bill of materials) cost for the implantable device and charging device does not exceed 200 USD which is excellent for quick prototyping of an implantable solution. The platform which was developed can be further extended with a range of sensors and actuators.

The future research will focus on direct use of the developed implant and charger device in research, specifically testing of the device in non-survival pig models. Also, further material research will be done so that the device will be biocompatible with regards to USP Class VI testing as well as fully hermetic, so it will be safe for long-term experiments and implantation in humans as well.

22 References

1. Exera, E. & Duodenovideoscope, I. I. Evis Exera Ii Duodenovideoscope Olympus Tjf Type Q180V. (1988). Available at: https://www.google.com/url?sa=t&rct=j&q=&esrc=s&source=web&cd=1&ved=0ahUKEwiDvLCd95nbAhVEIJoKHfU3CL4QFggqMAA&url=https%3A%2F%2Fwww.olympus.com.ru%2Fmedical%2Fru%2Fmedical_systems%2Fhidden%2Fdownload_jsp.jsp%3Flink%3D%2Fmedical%2Frmt%2Fmedia%2Fen%2Fcontent%2Fcontent_1%2Fdocuments_1%2Fmanuals_1%2FTJF-Q180V_Operation_Manual_20160401.pdf&usg=AOvVaw2G7_IDBtijajKQu8Hs4WP9. (Accessed: 10th May 2018)
2. Deb, S. *et al.* Development of innovative techniques for the endoscopic implantation and securing of a novel, wireless, miniature gastrostimulator (with videos). *Gastrointest. Endosc.* **76,** 179–184 (2012).
3. Sharata, A. *et al.* Technique of per-oral endoscopic myotomy (POEM) of the esophagus (with video). *Surg. Endosc.* **28,** 1333–1333 (2014).
4. Hajer, J. & Novák, M. Development of an Autonomous Endoscopically Implantable Submucosal Microdevice Capable of Neurostimulation in the Gastrointestinal Tract. *Gastroenterol. Res. Pract.* **2017,** 1–8 (2017).
5. Badillo, R. Diagnosis and treatment of gastroesophageal reflux disease. *World J. Gastrointest. Pharmacol. Ther.* **5,** 105 (2014).
6. Camilleri, M., Parkman, H. P., Shafi, M. A., Abell, T. L. & Gerson, L. Clinical Guideline: Management of Gastroparesis. *Am. J. Gastroenterol.* **108,** 18–37 (2013).
7. Soffer, E. Effect of electrical stimulation of the lower esophageal sphincter in gastroesophageal reflux disease patients refractory to proton pump inhibitors. *World J. Gastrointest. Pharmacol. Ther.* **7,** 145 (2016).
8. Medtronic Inc. Enterra ™ Therapy. (2012). Available at: https://manuals.medtronic.com/wcm/groups/mdtcom_sg/@emanuals/@era/@neuro/documents/documents/contrib_147120.pdf. (Accessed: 29th August 2017)
9. Soffer, E. E. Gastric Electrical Stimulation for Gastroparesis. *J. Neurogastroenterol. Motil.* **18,** 131–137 (2012).
10. Medtronic Inc. Investigation of the Spectrum Requirements for Advanced Medical Technologies. (1999). Available at: https://ecfsapi.fcc.gov/file/6520221065.pdf. (Accessed: 10th December 2017)
11. IEC. IEC 60601-1. (1986). doi:10.5594/J09750
12. European Parliament and of the Council. Council Directive 93/42/EEC. *Off. J. Eur. Union* 1–60 (2007). doi:2004R0726 - v.7 of 05.06.2013

13. Wheeler, H. A. Fundamental Limitations of Small Antennas. *Proc. IRE* **35,** 1479–1484 (1947).
14. Standard, H. E. Draft ETSI Ultra Low Power Medical Data Service (MEDS). **1,** 1–57 (2016).
15. Dove, I. Mathematics & Computer Science Analysis of Radio Propagation Inside the Human Body for in-Body Localization Purposes. (University of Twente, 2014).
16. Silicon Labs. Si4455 - easy to use, low current OOK/(G)FSK sub-GHz transceiver. 1–40 (2013). Available at: https://www.silabs.com/documents/public/data-sheets/Si4455.pdf. (Accessed: 26th March 2018)
17. Sýkora, J. *Teorie digitální komunikace*. (ČVUT Praha, 2002).
18. Peterson, W. & Brown, D. Cyclic Codes for Error Detection. *Proc. IRE* **49,** 228–235 (1961).
19. Lecture, D. & Last, N. C HAPTER 8 Viterbi Decoding of Convolutional Codes. **2011,** 87–102 (2012).
20. EternityForest. Ultra Fast Pseudorandom number generator for 8-bit. Available at: https://www.electro-tech-online.com/threads/ultra-fast-pseudorandom-number-generator-for-8-bit.124249/. (Accessed: 10th April 2018)
21. Rijmenants, D. The Complete Guide to Secure Communications with One Time Pad Cipher. *Cipher Mach. Cryptol.* 1–27 (2010).
22. Novotný, K. *Teorie elmag. pole I. Skriptum.* (ČVUT Praha, 1998).
23. Wire Gauge and Current Limits Including Skin Depth and Strength. Available at: https://www.powerstream.com/Wire_Size.htm. (Accessed: 14th May 2018)
24. Battery, P. L. CG-320A Pin-type Li-ion Battery. (2017). Available at: https://industrial.panasonic.com/content/data/BT/docs/edbd/pin/CG320A_DataSheet_EN%28WW%29_20170419.pdf. (Accessed: 20th May 2018)
25. Microchip Technology Inc. PIC16(L)F1717/8/9 Data Sheet. (2015). Available at: http://ww1.microchip.com/downloads/en/DeviceDoc/40001740B.pdf. (Accessed: 3rd February 2018)
26. Nexperia. RB521CS30L Schottky barrier rectifier. Available at: https://assets.nexperia.com/documents/data-sheet/RB521CS30L.pdf. (Accessed: 4th February 2018)
27. Nexperia. BZT52 series Single Zener diodes. Available at: https://assets.nexperia.com/documents/data-sheet/BZT52_SER.pdf.
28. Texas Instruments. TPS82740x 360nA I Q MicroSIP TM Step Down Converter Module for Low Power Applications. Available at: http://www.ti.com/lit/ds/symlink/tps82740b.pdf. (Accessed: 2nd February 2018)
29. Maxim Integrated. High-Efficiency LCD Boost with True Shutdown High-Efficiency

LCD Boost with True Shutdown. Available at: https://datasheets.maximintegrated.com/en/ds/MAX8570-MAX8575.pdf. (Accessed: 4th February 2018)

30. Semiconductor Components Industries, L. Rail-to-Rail Output Operational Amplifier. (2015). Available at: http://www.onsemi.com/pub/Collateral/NCS2004-D.PDF. (Accessed: 8th February 2018)
31. Joung, Y.-H. Development of Implantable Medical Devices: From an Engineering Perspective. *Int. Neurourol. J.* **17,** 98 (2013).
32. International Standardization Organization. ISO 10993-1, 'Biological evaluation of medical devices - Part 1: Evaluation and testing within a risk management process'.
33. ST Microelectronics Inc. LD1117 Adjustable and Fixed Low-Dropout Voltage Regulator. 1–44 (2013). Available at: http://www.ti.com/lit/ds/symlink/tlv1117-50.pdf. (Accessed: 10th February 2018)
34. FTDI Technology. Ft232R Usb Uart Ic. 1–40 (2008). Available at: http://www.ftdichip.com/Support/Documents/DataSheets/ICs/DS_FT232R.pdf.
35. Microchip Technology Inc. PIC16(L)F1782/3 Data Sheet. (2012). Available at: http://ww1.microchip.com/downloads/en/DeviceDoc/41579C.pdf. (Accessed: 20th August 2017)
36. ON Semiconductor. NCP5183, NCV5183 High Voltage , High and Low Side Driver. *Time* 1–14 (2008). Available at: http://www.onsemi.com/pub/Collateral/NCP5183-D.PDF. (Accessed: 9th February 2018)
37. ON Semiconductor. NVMFS5844NL 60 V , 61 A , 12 mW , Single N − Channel. Available at: https://www.onsemi.com/pub/Collateral/NTMFS5844NL-D.PDF. (Accessed: 1st February 2018)
38. Wakefield-Vette. ulTIMiFlux Thermal Gap Filling Pad. Available at: https://cz.mouser.com/datasheet/2/433/Wakefield-Vette Data Sheet ulTIMiFlux Final-1086223.pdf. (Accessed: 10th May 2018)